CHARACTERIZATION OF THE LOCAL ELECTRICAL ENVIRONMENT IN AN ELECTRICALLY-GUIDED PROTEIN PATTERNING SYSTEM INCORPORATING ANTIFOULING SELF-ASSEMBLED MONOLAYER

A Thesis

by

JINSEON PARK

Submitted to the Office of Graduate Studies of
Texas A&M University
in partial fulfillment of the requirements for the degree of

MASTER OF SCIENCE

August 2010

Major Subject: Physics

Characterization of the Local Electrical Environment in an Electrically-guided Protein Patterning System Incorporating Antifouling Self-assembled Monolayer

CHARACTERIZATION OF THE LOCAL ELECTRICAL ENVIRONMENT IN AN ELECTRICALLY-GUIDED PROTEIN PATTERNING SYSTEM INCORPORATING ANTIFOULING SELF-ASSEMBLED MONOLAYER

A Thesis

by

JINSEON PARK

Submitted to the Office of Graduate Studies of
Texas A&M University
in partial fulfillment of the requirements for the degree of

MASTER OF SCIENCE

Approved by:

Co-Chairs of Committee,	Winfried Teizer
	Wonmuk Hwang
Committee Member,	Glenn Agnolet
Head of Department,	Edward Fry

August 2010

Major Subject: Physics

ABSTRACT

Characterization of the Local Electrical Environment in an Electrically-guided Protein Patterning System Incorporating Antifouling Self-assembled Monolayer. (August 2010)

Jinseon Park, B.S., Texas A&M University

Co-Chairs of Advisory Committee: Dr. Winfried Teizer
Dr. Wonmuk Hwang

In earlier research in our lab, the manipulation of microtubules on gold patterned silicon wafers was achieved by E-beam lithography, Poly (ethylene glycol) self assembled monolayers (PEG-SAMs) and electrophoresis. To develop a technique for delicate single microtubule manipulation, further studies need to be done on PEG-SAMs and electrophoresis. As a foundation of this goal, we examined the electric field in an aqueous solution between two planar electrodes and the compatibility of the antifouling property of PEG-SAMs with the electric field. For this purpose, the distribution of microbeads was analyzed using a Boltzmann distribution. The amount of adsorbed microtubules on a PEG-SAM was examined to test the compatibility of the antifouling property of a PEG-SAM with concomitant exposure to electric field. It is shown that the product of the electric field and the effective charge of the microbead does not have a linear relation with the applied electric potential but an exponentially increasing function with respect to the potential. The antifouling property of the PEG-SAM was not retained after an exposure to the electric field.

DEDICATION

This thesis is dedicated to my parents, Jeaman and Kisoon, who have raised me with unconditional love, unstinting support, and faithful prayer. Thank you for all the love, support and prayer that you have given me.

ACKNOWLEDGEMENTS

I would like to thank my research advisors and committee members, Dr. Winfried Teizer, Dr. Wonmuk Hwang and Dr. Glenn Agnolet for their guidance throughout my study. Without you, my study would not have been possible. Thank you so much for a great experience. Thanks also go to Sung-Oh Woo, my labmate, for helping me with coursework and for his helpful discussions on my research for the last two years. I could not have made it through without your help and encouragement. I also thank my labmates for their friendships and support. It has been a great experience to spend my time with you all. Good luck to each of you in the future. Finally, thanks to my family for their never-ending love and support. I love you.

NOMENCLATURE

AFM	Atomic Force Microscopy
DI	Deionized
DIC	Differential Interference Contrast
FT-IR	Fourier Transform Infrared Spectroscopy
GMPCPP	Guanosine-5'-[(α,β)-methyleno]triphosphate
MIBK	Methyl Isobutyl Ketone
MPEOPS	2-[methoxypoly-(ethyleneoxy)propyl]-trimethoxysilane
MT	Microtubule
PEG-SAM	Poly(ethylene glycol) Self Assembled Monolayer
PMMA	Poly(methyl methacrylate)
QCM	Quartz Crystal Microbalance
SEM	Scanning Electron Microscopy
SIMS	Secondary Ion Mass Spectrometry
XPS	X-ray Photoelectron Spectroscopy

TABLE OF CONTENTS

Page

ABSTRACT iii

DEDICATION iv

ACKNOWLEDGEMENTS v

NOMENCLATURE vi

TABLE OF CONTENTS vii

LIST OF FIGURES ix

LIST OF TABLES xi

CHAPTER

I INTRODUCTION 1

1.1 Overview 1
1.1.1 Immobilization of Bio-molecules 1
1.1.2 PEG-SAMs and Electrophoresis as Immobilization Methods 2
1.2 Motivation 4

II ELECTROSTATIC SCREENING IN AN AQUEOUS SOLUTION . 6

2.1 Introduction 6
2.2 Background 7
2.2.1 Electric Potential between Two Planar Electrodes 7
2.2.2 Fluorescence Microscopy 9
2.2.3 Differential Interference Contrast (DIC) Microscopy 10
2.3 Materials and Methods 12
2.3.1 Microbeads Preparation 12
2.3.2 Electron Beam Lithography for Fabrication of Electrode 12
2.3.3 Electrode Preparation – Thermal Evaporation 14
2.3.3.1 Transparent Planar Electrode 14
2.3.3.2 Non-transparent Planar Electrode 16
2.3.3.3 Disk Micro-electrode 17

CHAPTER Page

2.3.4 Flow Cell Preparation 18
2.3.5 Mobility Test of Microbeads under Electric Potential 19
2.3.6 Pattering of Microbeads on a Disk Micro-electrode 19
2.3.7 Photobleaching Test 20
2.3.8 Z-series Image Acquisition Using Fluorescent Microscopy . 22
2.3.9 Distribution Assay – Number Concentration 23
2.4 Results and Discussion 23
2.4.1 Motility of Microbeads under Influence of Electric Field 23
2.4.2 Pattering of Microbeads on a Disk Micro-electrode 24
2.4.3 Photobleaching Test 25
2.4.4 Distribution of Microbeads under Influence of Electric Potential 28
2.4.4.1 Distribution of Microbeads without an Electric Potential 28
2.4.4.2 Boltzmann Distribution of Microbeads 30
2.4.4.3 Electric Potential Dependence 32
2.4.4.4 Time Dependence 36
2.5 Conclusion 39

III COMPATABILITY OF ANTIFOULING PROPERTY OF PEG-SAM WITH ELECTRIC FIELD 40

3.1 Introduction 40
3.2 Background – Antifouling Property of PEG-SAM 41
3.3 Materials and Methods 42
3.3.1 Electrode Preparation 42
3.3.2 PEG-SAM Formation 42
3.3.3 Flow Cell Preparation 43
3.3.4 Exposure to E-field 43
3.3 5 Microtubule Preparation 43
3.3.6 Antifouling Property Assay Using Microtubules 44
3.4 Results and Discussion 44
3.5 Conclusion 46

IV SUMMARY 47

REFERENCES 49

VITA 51

LIST OF FIGURES

FIGURE		Page
1.1	Previously achieved reversible MT adsorption on a passivated disk electrode	3
2.1	Electrostatic screening in a flow cell	9
2.2	Images taken by the fluorescence microscope	10
2.3	Comparison of DIC and fluorescence microscope images	11
2.4	Electron beam lithography procedure	13
2.5	Experimental setup for a thermal evaporation system	15
2.6	The fabricated disk micro-electrode on a silicon wafer	17
2.7	Experimental setup for a flow cell	18
2.8	Photobleaching of the microbeads	21
2.9	Scheme of the image acquisition process	23
2.10	Mobility test of the microbeads under an electric potential	24
2.11	Reversible patterning of the microbeads	25
2.12	Characterization of the photobleaching phenomenon	26
2.13	Photobleaching test at fixed height	27
2.14	Distribution of the microbeads without an electric potential	29
2.15	The distribution of the microbeads	31
2.16	Log of the number concentration of the microbeads	31
2.17	Potential dependence of the distribution	33
2.18	Log of the number concentration (potential dependence)	33

FIGURE Page

2.19 Calculated values for ‘qE’ 35

2.20 Time dependence of the distribution 37

2.21 Log of the number concentration (Time dependence) 38

3.1 Adsorption of microtubules on the electrically treated PEG-SAM..... 45

LIST OF TABLES

TABLE Page

2.1 Types of Electrodes 14

2.2 Time table of the applied electric potential 19

2.3 Calculated values for ‘qE’ from Figure 2.18 34

CHAPTER I

INTRODUCTION

1.1 Overview

1.1.1 Immobilization of Bio-molecules

Techniques for the immobilization of bio-molecules, including proteins and peptides, on a patterned surface have been of great interest for bio and life scientists. These techniques have been developed in various manners achieving a resolution of patterned regions below the micron size.[1] This leads to great potential of these techniques to be utilized in two major areas: (1) bio-engineering such as biosensors and (2) scientific research to understand the nature of proteins. Various techniques for immobilizing bio-molecules can be classified into either direct or indirect approaches. While direct immobilization methods involve direct contact between bio-molecules and particular regions of the substrate, indirect immobilization methods exploit intermediate driving forces to attract or grab bio-molecules onto patterned regions. To achieve indirect immobilization of bio-molecules onto an intended area, a two-step process is considered. First, it must be ensured that there are no bio-molecules on the substrate except in the intended region. In other words, any non-specific fouling of bio-molecules on the substrate

---

This thesis follows the style of *Nano Letters.*

must be prevented. Bio-molecules are usually adsorbed onto the substrate non-specifically due to hydrophobic and electrostatic interactions with the substrate. Therefore, the surface of the substrate should be functionalized in order to exert antifouling properties against bio-molecules. Although there are many well-developed marine antifouling coatings, those are not appropriate for laboratory use at the size of microns. This is because most of them are developed for large-scale commercial purposes, such as paint.[2] Recently, however, as the demand for micro-scale antifouling techniques in laboratory use increases, diverse ultra-thin passivation coating methods have been considered such as carbohydrate surface modification or poly(ethylene glycol), passivating protein layers and surfactant additives. The second step deals with the driving force to achieve adsorption of the bio-molecules on the designed area. The most commonly used method is chemisorption of targeted bio-molecules on patterned receptors.[3-5] The driving force for this method is chemical bonding between atoms. One of the drawbacks of this method is the irreversibility of the immobilization. However if we use electrophoresis as the driving force to accomplish the immobilization of the target molecule on an electrode, it is possible to attract target molecules in a reversible manner.

1.1.2 PEG – SAMs and Electrophoresis as Immobilization Methods

Fabrication of microtubules, a type of cytoskeleton found in the human body, has been achieved in our laboratory.[6] Microtubules have negative charge in neutral pH and a cylindrical structure with a diameter of 25 nm and variable lengths from 200 nanometers

to 25 micrometers. In order to achieve micro-size manipulation of microtubules, an indirect immobilization method was employed. Poly(ethylene glycol) self assembled monolayers (PEG-SAMs) and electrophoresis have been selected for functionalizing the silicon wafer surface to have an antifouling property and exploiting the driving force to attract microtubules to a patterned gold microelectrode. To pattern a gold disk-microelectrode on a silicon wafer, electron beam lithography was used because it has relative advantages in terms of resolutions despite its long exposure time and low throughput.

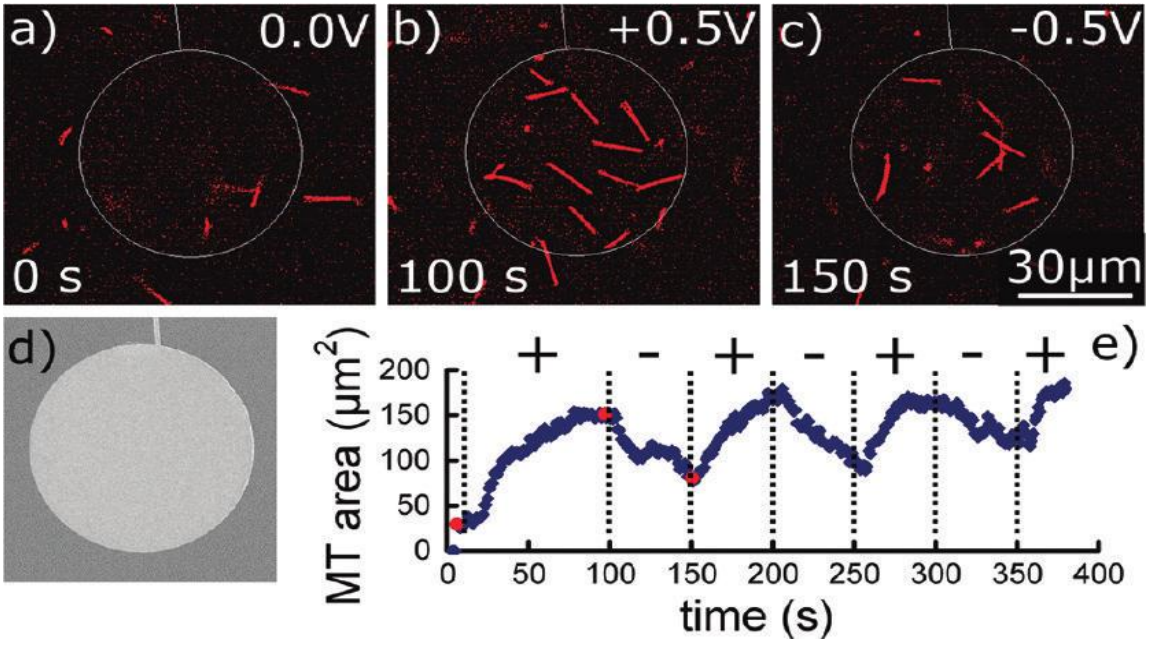

Figure 1.1 Previously achieved reversible MT adsorption on a passivated disk electrode. (a) Initially, the electrodes are grounded, and there is no adsorption. (b) MTs are concentrated on the disk for 100 s at + 0.5 V DC. (c) Potential is then reversed to drive MTs away for 50 s. White lines indicate edges of electrode. (d) Scanning electron microscopy (SEM) image of a disk electrode. (e) Plot of MT area in μm^2 (converted from pixel area) covered by MTs on the electrode as a function of time with + 0.5 and - 0.5 V applied alternately; images a-c are taken from the same experiment and are indicated in the plot with a red dot. From Ref. 6.

By combining these three methods (PEG-SAM, E-beam lithography and Electrophoresis), the reversible adsorption of microtubules on a patterned gold microelectrode has been successfully observed in previous studies (Figure1.1). For this experiment, an electric potential up to 1.0V was applied between two parallel electrodes that are 60 micrometers apart. The study has shown a very promising result since it revealed the potential to make bio-tracks where motor proteins, called kinesin, can walk along to transport cargo.[7] However, we still have to improve the individual microtubule alignment to make an elaborate bio-track.

1.2 Motivation

As discussed above, the foundation for the fabrication of microtubules on artificially designed substrates has been established by performing reversible adsorption of microtubules. However, in order to align and manipulate a single microtubule to construct a bio-track, further studies have to be carried out to understand the true mechanism of the manipulation of a system composed of electrophoresis and PEG-SAM. First, the electric field that is formed in an aqueous solution by applying an external electric potential has to be studied. A calculation of the electric field in a vacuum environment is straightforward, but it is not as obvious in the case of an aqueous solution despite the simple geometry. This is because ions in an aqueous solution can cause electrostatic screening.[8-10] It is important to understand the electrostatic screening in an aqueous solution because it can have an influence on the effective charge of charged particles as well as an electric field. Since the driving force upon applying an electric

potential is determined by the electric field and the effective charge of the particles, without a reasonable understanding of the electrostatic screening, elaborate manipulation of microtubules is difficult. In this study, the influence of the electrostatic screening on both an electric field and an effective charge of particles in an aqueous solution was examined by analyzing the distribution of charged microbeads under the influence of an external electric potential. Secondly, the compatibility of PEG-SAMs and electric field should be verified to combine those methods in a manipulating system. Although SAMs comprise one of the most popular research areas in biochemistry since the 1980s, and have been actively studied for several decades, there are only few reports about the influence of an electric field on a SAM's structure and functionality.[11-12] In this study, the resilience of the antifouling properties of the PEG-SAM upon exposure to electric field was studied using microtubules.

CHAPTER II

ELECTROSTATIC SCREENING IN AN AQUEOUS SOLUTION

2.1 Introduction

In order to achieve fine control of charged particles using an electric field as a driving force in an aqueous solution, studies about the electrostatic screening have to be done before other characterization of a protein manipulation system. The electrostatic screening is caused by ions in an aqueous solution and because the ions have mobility, application of an external electric potential will cause considerable changes in the electrostatic screening, and eventually, it will affect the electric field and effective charge of the particles in an aqueous solution. To study the influence of the electrostatic screening on an electric field and the effective charge of particles, microbeads were used in a model study. In this chapter, mainly three types of experiments were performed; (1) A mobility test of the microbeads, (2) Reversible patterning of the microbeads, (3) Distribution of the microbeads under an electric potential. In experiment (1), by testing the mobility of the microbeads under an electric potential using differential interference contrast (DIC) microscopy, the charge of the microbeads was verified. In experiment (2), reversible pattering of the microbeads on a disk micro-electrode was achieved and observed using fluorescence microscopy. In experiment (3), the relationship between the applied electric potential, the resulting electric field and the effective charge of the microbeads was examined by investigating the distribution of the microbeads between

oppositely charged electrodes using fluorescence microscopy and the NIS Elements software. In order to analyze the distribution, the Boltzmann distribution was employed.

2.2 Background

2.2.1 Electric Potential between Two Planar Electrodes

An electric field appears between two electrodes of opposite polarity and the electric potential can be calculated by solving Laplace's equation with boundary conditions.

$$\frac{d^2\phi(x)}{dx^2} = 0$$

$$\phi(x): \text{electric potential}$$

If charge is distributed inside the medium, the electric potential follows the solution of Poisson's equation. Poisson's equation has an additional term, $\rho(x)$, which stands for the charge density in the space of interest.

$$\frac{d^2\phi(x)}{dx^2} = \frac{\rho(x)}{\varepsilon_0}$$

$$\varepsilon : \text{permittivity}, \rho(x): \text{charge density}$$

Furthermore, if the charged species are mobile and are in equilibrium in the medium, the poisson-Boltzmann equation is used to calculate the electric potential inside the medium.

$$\frac{d^2\phi(x)}{dx^2} = -\frac{1}{\varepsilon}\sum_i z_i q \rho_{i\infty} \exp\left[-\frac{z_i q \phi(x)}{k_B T}\right]$$

z_i : valence of the i$_{th}$ ion, q : charge of a proton, $\rho_{i\infty}$: bulk concentration of the i$_{th}$ ion
k_B : Boltzmann constant, T : temperature

The Poisson-Boltzmann equation is a modified Laplace's equation for describing electrostatic interactions between molecules in ionic solutions. In an ionic solution surrounded by substrates with surface charges, counterions will be accumulated on the surface of a substrate by electrostatic interaction resulting in a phenomenon known as electrostatic screening. Electrostatic screening leads to a decay of the electric potential inside the medium, and the decay length, called the Debye length, can be calculated by solving the Poisson-Boltzmann equation. However, for a complex system composed of ions and charged particles called macro-ion, the calculation becomes complicated (Figure 2.1). Thus, in this study, an experimental analysis of the distribution of the charged particles is performed to estimate the electric potential inside the flow cell. The microbeads, which are used as model charged particles in this study, have a diameter of 0.5 micron and a negative charge when they are dissolved in aqueous solution. By counting the number of microbeads and plotting their distribution, the electric field can be calculated because they follow the Boltzmann distribution.

$$\rho(x) = \rho_0 e^{-\beta\varepsilon} = \rho_0 e^{-\frac{q\phi(x)}{k_B T}}$$

$\rho(x)$: number concentration, k_B : Boltzmann constant
q : effective charge of the microbead, $\phi(x)$: electric potential

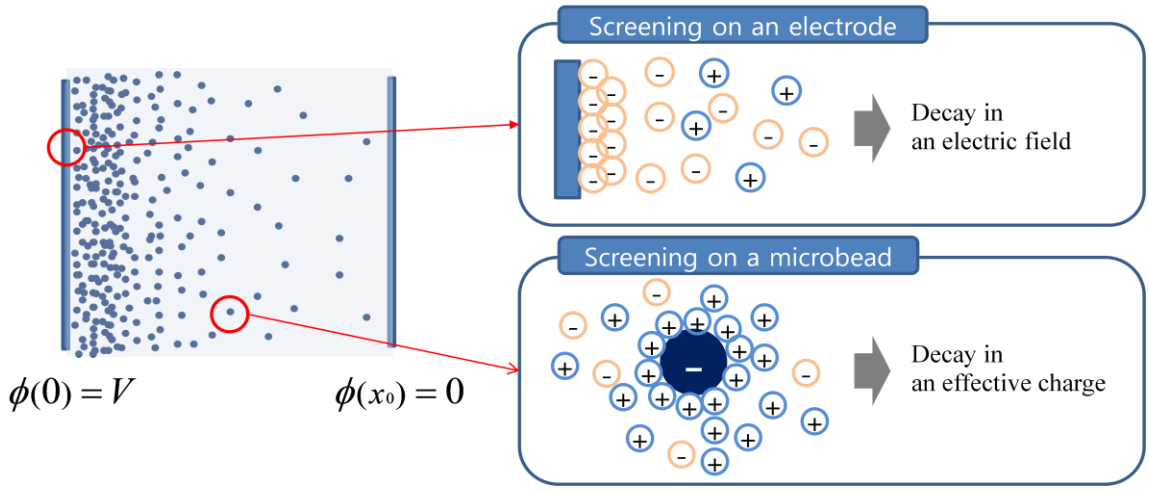

Figure 2.1 Electrostatic screening in a flow cell. The electrostatic screening occurs on an electrode and a microbead caused by self-ionized ions in an aqueous solution.

2.2.2 Fluorescence Microscopy

Fluorescence microscopy is widely used in biology and bio-engineering to track positions of specially labeled organic or inorganic substances. In order to use fluorescence microscopy, fluorophores such as a fluorescein and a green fluorescent protein are used to label the specimen. The labeled specimen is then exposed to an excitation light that is absorbed by the fluorophores, and subsequently, fluorophores in the specimen emit light at a longer wavelength than the excitation light. An appropriate combination of a light source and proper excitation and emission filters are required for the efficient use of a fluorescence microscope. In this study, fluorescence microscopy was used to detect the microbeads inside the flow cell which include fluorophores. In fluorescence microscopy, photobleaching of the fluorephores should be taken into account to get valid data. Photobleaching refers to a phenomenon in which emission light of the fluorophore gets weaker during an exposure process due to continuing

illumination. In this study, the photobleaching phenomenon was examined and an appropriate protocol was developed to minimize the effect of the photobleaching on the results. Figure 2.2 shows the images of the microbeads and the microtubules taken by the fluorescence microscope.

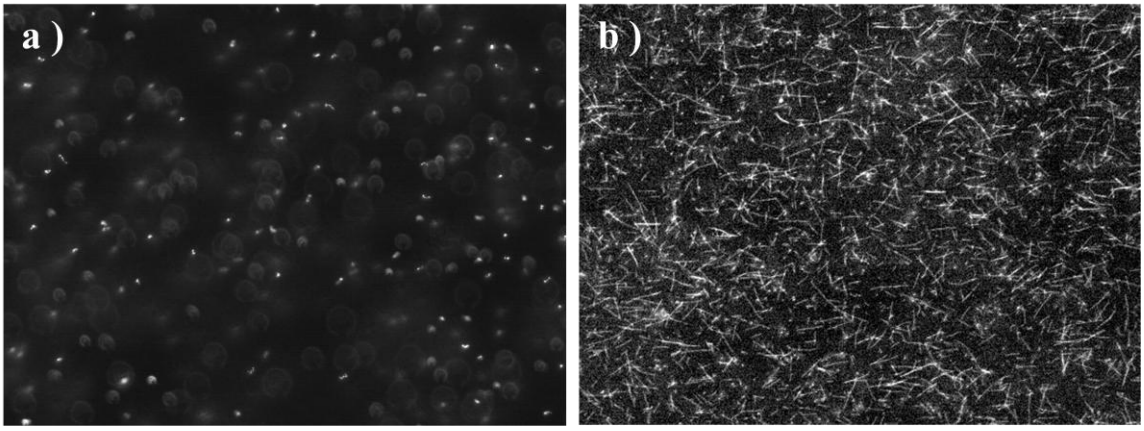

Figure 2.2 Images taken by the fluorescence microscope. 20X objective lens was used. a) Microbeads of a number concentration of 1.5×10^{6} / ml (1×10^{-5} % w/v). b) Microtubules of a concentration of 125nM..

2.2.3 Differential Interference Contrast (DIC) Microscopy

Microbeads used in this research are optically transparent and thus it is impossible to observe them using an ordinary optical microscope which detects the differences in the constrast or color. For this reason, a fluorescence microscope and fluorescent microbeads were used in this research. DIC microscopy can be a possible alternative for observing transparent substances (Figure 2.3). It is because the DIC microscopy utilizes differences in the optical path length of adjacent areas of the substance to generate an image. The optical path length is the product of the refractive index and the geometric path length through the specimen. The lighting scheme for the DIC microscopy is

relatively complex. Unpolarized illumination light is polarized through a polarizing filter, and the polarized light is separated by a Wollaston prism into two rays which are rotated so they are crossing each other at right angles. When the two rays pass through a condenser, they are focused on the specimen. The notable thing in this step is that the two rays pass through two adjacent points. That is, they are not aligned but separated by a slight distance to each other in a certain direction. Therefore, the two rays passing through the two adjacent points experience different degrees of phase shift which is determined by the optical path length (the product of refractive index and thickness) of the two adjacent paths. After traveling through an objective lens, they arrive at a second Wollaston prism and are recombined into an identically polarized ray. The recombination of the two rays results in interference according to the optical path difference between the adjacent paths, and the interference results in the contrast of the image. Eventually, the gradient of the optical path of the specimen determines the contrast.

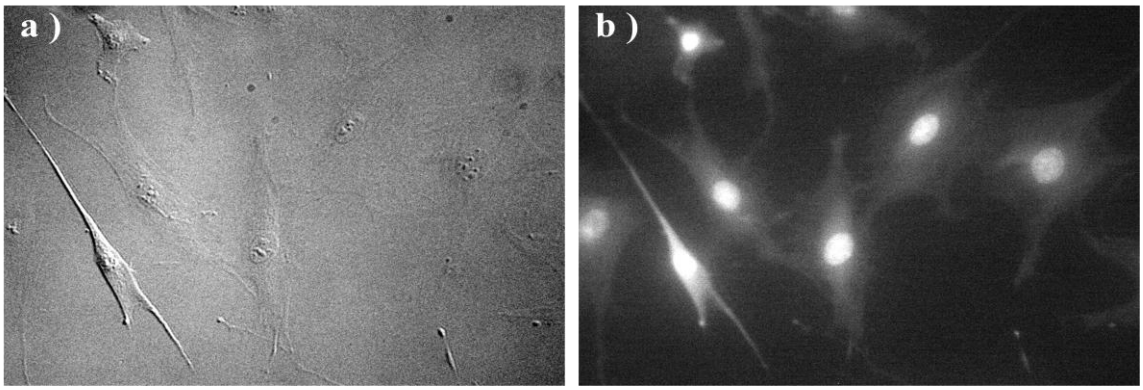

Figure 2.3 Comparison of DIC and fluorescence microscope images. Fibroblast cells were used as specimen and they have fluorophores in their nucleus. a) DIC microscope image. b) Fluorescence microscope image.

2.3 Materials and Methods

2.3.1 Microbeads Preparation

The microbeads (Fluorescent Purple Particles, FP-0562-2) were purchased from Spherotech, Inc. The microbeads, polystyrene microspheres, have a diameter of 0.4-0.6 μm, and its original number concentration was 1.5×10^{11} / ml (1.0 % w/v). In order to make the appropriate concentration for the experiment, the original solution had to be diluted 1000 times with deionized (DI) water. The final number concentration was 1.5×10^{8} / ml (1×10^{-3} % w/v). This diluted microbead solution in a microtube was placed in a vortexer and sonicator for 5 seconds each to disperse the microbeads in the solution. The microbead solution was stored in a dark drawer to prevent photobleaching from occurring. In an aqueous solution, the microbeads have negative charge because they have sulfonate groups ($R\text{-}SO_2O^-$) on the surface since potassium persulfate ($K_2S_2O_8$) is used in the process making the microbeads. (The company doesn't have information on how many ions are on the surface of the microbead) Under the influence of an external electric field the microbeads distribute according to the applied electric potential.

2.3.2 Electron Beam Lithography for Fabrication of Electrode

To make the disk-microelectrode, electron-beam lithography was used (Figure 2.4). The procedure for electron-beam lithography was adapted from our previous research.[6] It consists of three steps, (1) spin-coating of electron-beam resist on a silicon wafer (2) electron-beam writing (electron-beam exposure) and (3) developing. First a silicon wafer

is cut to 1x1.5 cm^2 to be placed on the electron microscope stage. After cutting the silicon wafer, we cleaned it according to the standard cleaning protocol which is composed of sonication of a cleaved silicon wafer in acetone for five minutes, followed by rinsing with acetone and isopropanol and drying with nitrogen gas. After the cleaned silicon wafers were placed on a hot plate at 200 ºC for complete drying, a few drops of electon-beam resist (PMMA (poly(methyl methacrylate)), 3% w/v in chlorobenzene) were placed on the wafer. After spinning for 50 seconds at 4000 rpm, it was placed on a hot plate (160 ºC) for 90 seconds. For e-beam writing we used a JEOL 6460 electron microscope that is controlled by Nano Pattern Generating Software (JC Nabity). Usually, four pieces of silicon wafers sized in 1x1.5 cm^2 can be placed on the stage so that we could sequentially expose them to write patterns by moving the stage and focusing on each silicon wafer without venting and replacing the silicon wafers. The electron-beam exposure process took a couple of minutes for each silicon wafer.

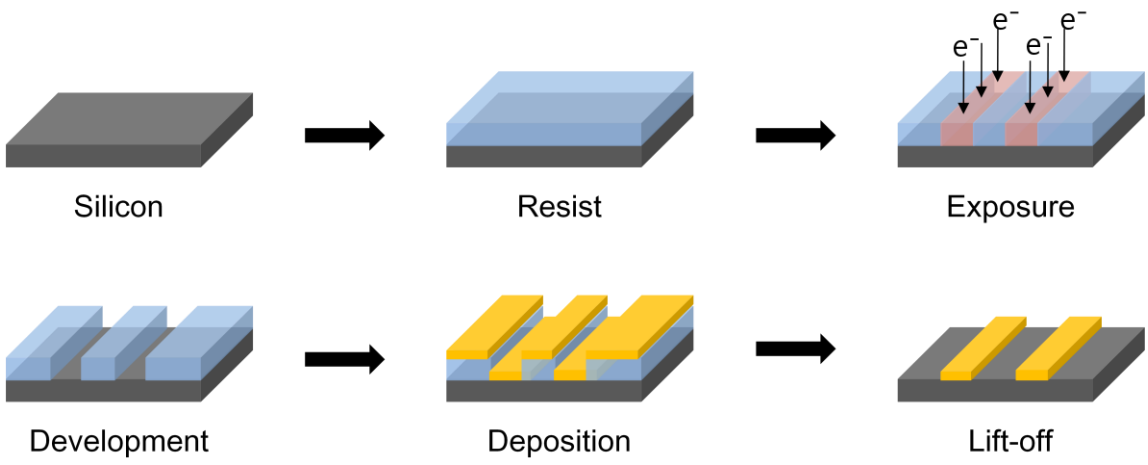

Figure 2.4 Electron beam lithography procedure. A resist layer was formed by using a spin-coater and thermal evaporation technique was exploited to deposit gold on the substrate.

Patterned silicon wafers were then submerged in developer, MIBK (methyl isobutyl ketone) in isopropanol (1:3), for 70 seconds followed by rinsing with isopropanol. After developing, the pattern on each silicon wafer was verified with an optical microscope.

2.3.3 Electrode Preparation - Thermal Evaporation

2.3.3.1 Transparent Planar Electrode

In this research, a flow cell was formed with two electrodes: the top and the bottom electrodes. Based on the purpose and the type of microscope used, an appropriate electrode type was selected for the top and the bottom electrodes respectively from the three options: transparent, non-transparent and disk micro-electrode (Table 2.1). In all experiments, a transparent electrode was used as the bottom electrode, because an inverted microscope was used in this research.

Table 2.1 Types of electrodes. For all the cases, a transparent electrode was used as the bottom electrode. In the experiment for checking the mobility of the microbeads under the influence of an external electric potential, a transparent electrode was used as the top electrode. A disk micro-electrode on a silicon wafer was used to obtain the patterning of the microbeads; and a non-transparent electrode was used to observe the distribution of the microbeads.

Purpose	Mobility of Microbeads	Pattering of Microbeads	Distribution of Microbeads
Microscope	DIC	Fluorescence	Fluorescence
Top electrode	Transparent	Disk Micro-eletrode	Non-transparent
Bottom electrode	Transparent	Transparent	Transparent

Because the objective lens was located below the stage, the bottom electrode should be transparent in order to allow the observation through it whether a DIC microscopy or a fluorescence microscopy was utilized. When DIC microscopy was used, the top electrode should also be transparent because an illumination light must penetrate the flow cell to make the differential interference contrast image. In order to fabricate electrodes, a thermal evaporation technique was used (Figure 2.5). To make the transparent electrode, a glass coverslip was used as a base substrate. To clean the substrate, the glass cover slip was put in a glass beaker filled with acetone and the beaker was placed in a sonicator for 5 minutes. After sonication, substrates were rinsed with fresh acetone and isopropanol followed by drying with nitrogen gas.

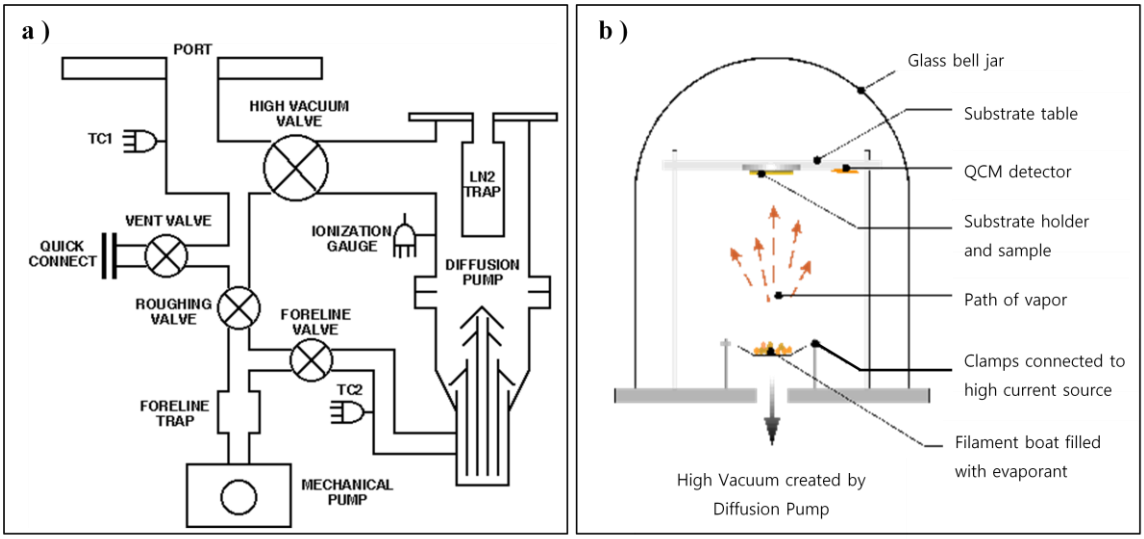

Figure 2.5 Experimental setup for a thermal evaporation system. a) The thermal evaporation system including mechanical, diffusion pump and vacuum gauges [source; http://mse.cornell.edu/mse/undergrad/lab/dp_sys.gif]. b) Composition of an evaporation chamber (bell jar) [source; http://www.betelco.com/sb/phd/ch3/f3-9.gif].

Cleaned substrates were attached to a sample holder of a thermal evaporation system, and the evaporation chamber (bell jar) was closed. A mechanical pump was used to make a low vacuum and a high vacuum was achieved by using a diffusion pump. When the vacuum level reached 5×10^{-6} Torr, a chromium bar and a boat holding a piece of gold were sequentially heated to evaporate them. The thickness of the deposited metal was estimated by a quartz crystal microbalance (QCM) monitor. For a transparent electrode, 1 nm of chromium (as an adhesion layer) and 4 nm of gold were deposited on a glass cover slip.

2.3.3.2 Non-transparent Planar Electrode

In the experiment for examining the distribution of the microbeads using a fluorescence microscope, a non-transparent electrode was used as the top electrode. In order to make the non-transparent electrode, a silicon wafer was used as the base substrate. The reason for using a non-transparent electrode as the top electrode is that the non-transparent silicon wafer can protect the microbeads from photobleaching and a glass coverslip would be too fragile to use. Photobleaching is the loss of emission light of fluorophores due to continuing illumination and will be discussed in subheading 2.3.7 and subheading 2.4.3 in detail. The silicon wafer was cut into the appropriate size (1 x 2 cm^2), and its fabrication process was identical to that of the transparent electrode except for the thicknesses of chromium and gold. In the fabrication of the non-transparent electrode, 3 nm of chromium and 12 nm of gold were deposited on a silicon wafer.

2.3.3.3 Disk Micro-electrode

In the microbead patterning experiment, a disk micro-electrode was used as the top electrode (Figure 2.6). To fabricate the disk micro-electrode, a silicon wafer substrate patterned with PMMA was prepared using e-beam lithography. Using a thermal evaporation method, 3nm of chromium and 12nm of gold were deposited on the patterned silicon wafer. To complete the disk micro-electrode on the silicon wafer, a lift off process was required to remove the remaining PMMA on the substrate. For this, the substrates were submerged in a beaker filled with acetone for 30 minutes. After 30 minutes, the beaker was placed in a sonicator for three seconds, and then the substrates were rinsed with acetone and isopropanol followed by drying with nitrogen gas.

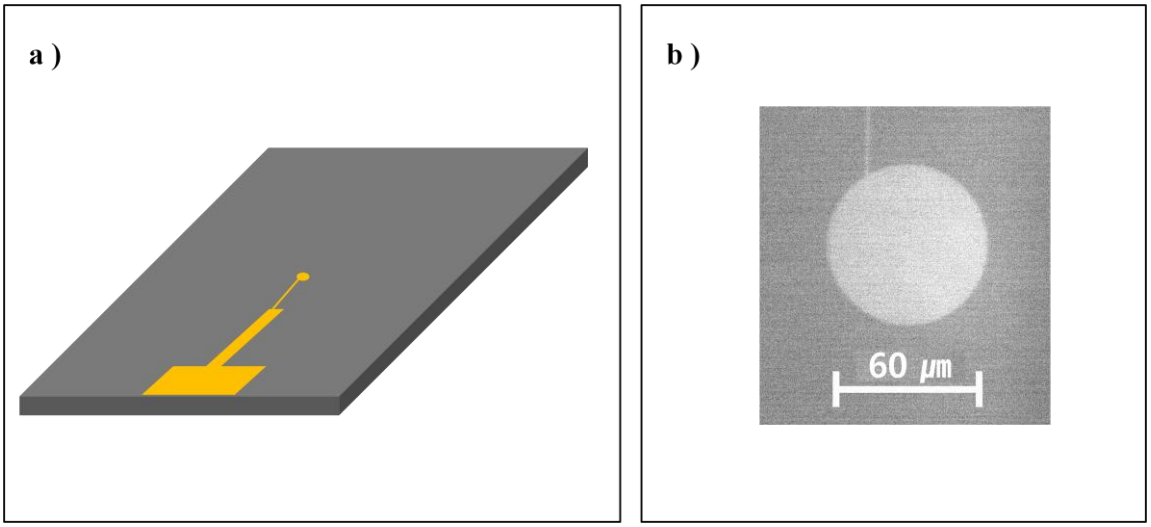

Figure 2.6 The fabricated disk micro-electrode on a silicon wafer. The diameter of the disk-electrode is 60 µm. a) Illustration of patterned silicon wafer. The disk-electrode is connected to a broader part through a thin line with width of 1 µm to make contact with a wire connecting to the power supply. b) A fluorescent image of the disk-electrode.

2.3.4 Flow Cell Preparation

In this study, an image acquisition system was composed of a power supply, a flow cell and the DIC or fluorescence microscope (Figure 2.7). The Flow cell consists of two electrodes made by thermal evaporation, strips of double-sided tape and two wires to connect to the power supply. The transparent electrode was placed on a surface with the chromium and gold coated side facing up. Strips of double sided tape were attached on the electrode 2-3 mm apart in a parallel direction. By attaching several strips, a number of cells can be made simultaneously. After attaching the strips of tape, the appropriate electrode selected based on the type of experiment was placed on the tape with the metal coated side facing downward. In this way, a flow cell with a height of 60 microns and a width of 2-3 millimeters was made. Two wires were connected to each electrode using silver paint. Vacuum grease was applied on both ends of the flow cell after introducing a solution to prevent evaporation and lateral flow of the solution.

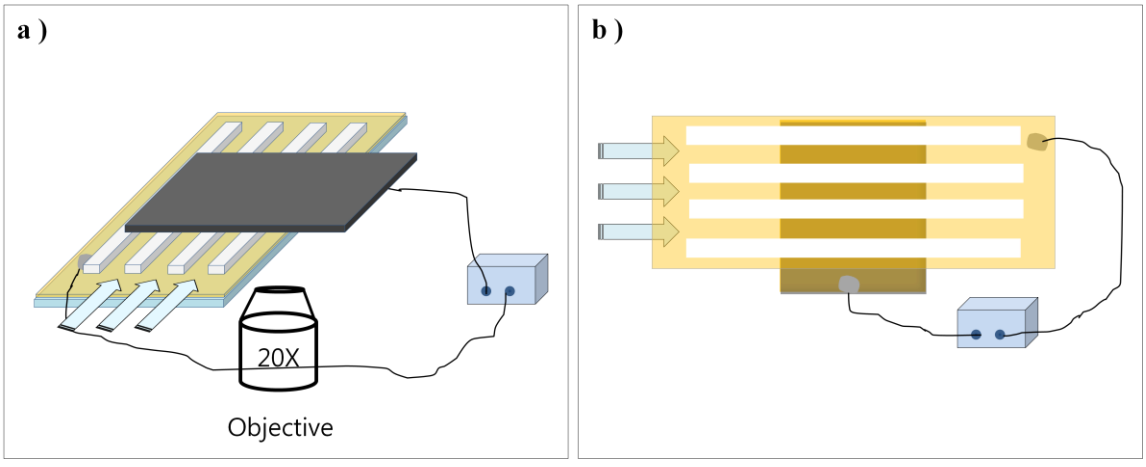

Figure 2.7 Experimental setup for a flow cell. a) The flow cell consists of two planar electrodes and strips of double sided tape. b) Illustration viewed from the bottom.

2.3.5 Mobility Test of Microbeads under Electric Potential

The mobility test was carried out to check the polarity of the microbeads. A DIC microscope was used in the mobility test, and a flow cell was made with two transparent electrodes. After introducing the microbead solution into the flow cell, the power supply was connected. The focal plane was placed slightly away from the top electrode using a 100X objective lens, and next, an electric potential was applied between the two planar electrodes. The test lasted for 60 seconds, in which +1.0 V and -0.5 V were applied for 10 seconds respectively in alternation (Table 2.2). In other words, +1.0V was applied for the first 10 seconds, and -0.5V for the next 10 seconds, and then followed by +1.0 V for the next 10 seconds and so on. The positive electric potential corresponds to the top electrode to be polarized positively, while a negative electric potential made the top electrode negatively polarized. The whole process was observed using a digital camera and recorded as a video file.

Table 2.2 Time table of the applied electric potential. +1.0 V and -0.5 V were applied for 10 seconds respectively in alternation between two planar electrodes.

Time(s)	0-10	10-20	20-30	30-40	40-50	50-60
Applied Potential(V)	+ 1.0V	- 0.5V	+ 1.0V	- 0.5V	+ 1.0V	- 0.5V

2.3.6 Patterning of Microbeads on a Disk Micro-electrode

Reversible patterning of microbeads on a disk micro-electrode was carried out using a flow cell composed of a transparent and a patterned disk micro-electrode as the bottom and the top electrode respectively. A fluorescence microscope was employed to observe

the flow cell. After introducing the microbead solution into the flow cell and connecting the power supply, the disk micro-electrode on the top substrate was chosen as the focal plane using a 20X objective lens and an electric potential was applied between the two electrodes. The time table for the applied electric potential was the same as was used in the experiment above (subheading 2.3.5). The test lasted for 60 seconds, in which +1.0 V and -0.5 V were applied for 10 seconds respectively in alternation. A positive electric potential corresponds to the top electrode being polarized positively. The images were taken at the end of the application of each reversed potential.

2.3.7 Photobleaching Test

When a fluorescence microscope is utilized, photobleaching of fluorophores should be considered to get valid information. Photobleaching refers to a phenomenon in which the emission light of the fluorophore gets weaker during an exposure process due to continuing illumination. The weakening of the emitted light by photobleaching cannot be recovered and can affect the measured quantity of the microbeads since the measured intensity of the emitted light determines the number of detectable microbeads. If a microbead has a high intensity of emission light, it can be detected in a wide range of focal planes, but if the microbead has low intensity, it can be detected only in a narrow range of focal planes (Figure 2.8). Therefore, in order to get reliable experimental data, it is important to verify how fast photobleaching will proceed and how much it will affect the measured results. In order to test the photobleaching, a series of images were taken over time at the middle of the flow cell under continuous exposure of excitation light.

First, the prepared microbead solution was introduced into the flow cell and both ends of the flow cell were sealed with vacuum grease to prevent lateral flow of the solution. The flow cell filled with the microbead solution was then placed on the stage of the fluorescence microscope. After focusing on the middle of the flow cell, the solution was exposed to an excitation light for 10 minutes and a series of images was taken at intervals of 10 seconds. The total number of the images was 60, and the whole test was repeated 5 times and averaged. Each series of images was taken using a new flow cell with fresh microbead solution. An automatic image acquisition tool in the NIS Elements software was used to get the series of images at intervals of 10 seconds. Emitted light from the microbeads was detected using a digital camera and was analyzed using the NIS elements software.

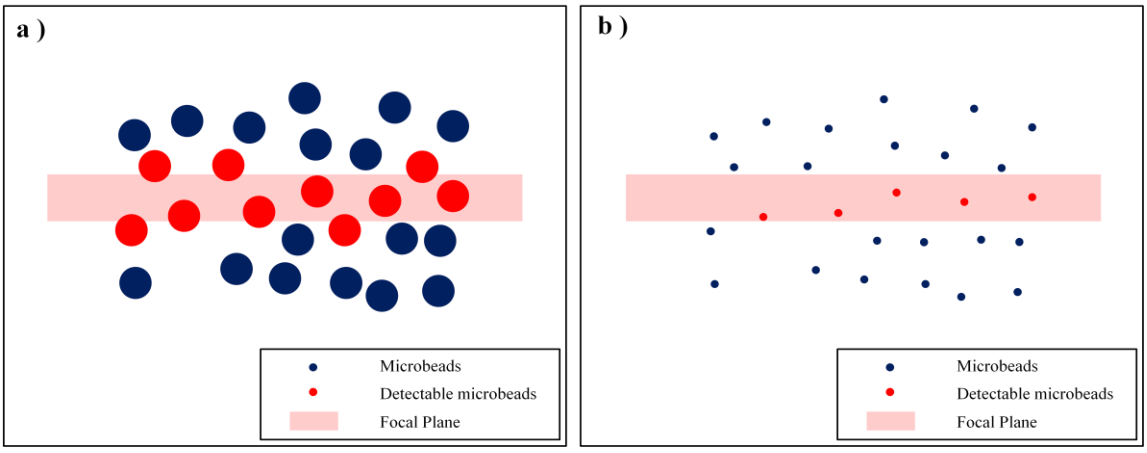

Figure 2.8 Photobleaching of the microbeads. The intensity of the emitted light and the detected number of microbeads are reduced after photobleaching. a) The microbeads have a high intensity of emitted light and result in a larger detectable radius of the fluorescent microbead. b) After some amount of exposure, photobleaching occurs on the microbeads. The microbeads have a low intensity of emitted light which results in a shrinking of the detectable radius of the fluorescent microbead.

2.3.8 Z-series Image Acquisition Using Fluorescence Microscopy

To examine the distribution of microbeads under an external electric potential, a Z-series of images were taken between two polarized electrodes at a fixed point (Z-direction was the direction of the applied electric potential). The Z-series images were composed of 11 images at intervals of 5 microns from the top electrode. The first image was taken at a distance of 5 microns from the top electrode and the last image was taken at the distance of 55 microns (Figure 2.9). After introducing the microbead solution to the flow cell, it was sealed with vacuum grease, and then placed on the stage of the fluorescence microscope. Copper wires which were already attached on both electrodes were connected to a power supply and the electric potential between the two electrodes was increased at a rate of 0.01V/s until it reached the desired voltage. After 5 minutes, the microbead solution was illuminated with excitation light for 5 minutes to reduce the photobleaching rate (The reason for this will be discussed in subheading 2.4.3 with the experimental results). 10 minutes after applying the electric potential, Z-series images were taken. The automatic image acquisition tool in NIS elements software was used and each image was taken every 20 seconds. During the 20 seconds, the focal length was changed by 5 microns by turning the focus knob and a shutter which blocks excitation light from the light source was opened only when the image was taken to minimize photobleaching of the microbeads. It took 3 minutes and 20 seconds to take one series of images. The emitted light from the microbeads was detected by a digital camera and was analyzed by the NIS Elements software.

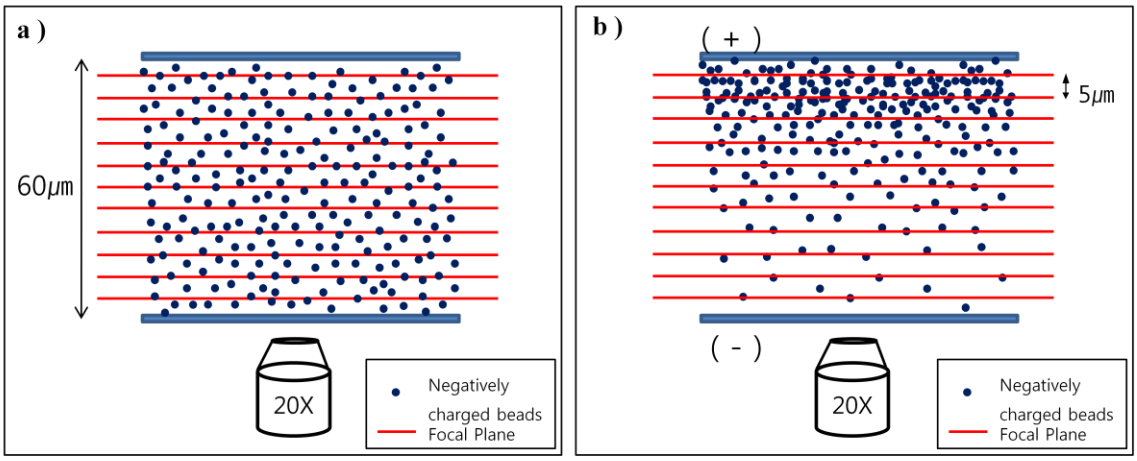

Figure 2.9 Scheme of the image acquisition process. Eleven images are taken across the flow cell from the top to the bottom at fixed location by changing the focal plane at intervals of 5 μm. a) Two electrodes are short-circuited and a uniform distribution of the microbeads was confirmed without electric potential. B) the electrodes have opposite polarity and negatively charged microbeads move to a positively charged surface.

2.3.9 Distribution Assay - Number Concentration

To measure the distribution of the number concentration along the Z-direction, 11 images were taken at fixed location but with varying focal lengths. Each image was analyzed using the NIS element software to count the number of microbeads in each image. To obtain the number counting process we had to determine the proper threshold value for intensity, diameter and area to recognize respective microbeads.

2.4 Results and Discussion

2.4.1 Motility of Microbeads under Influence of Electric Field

The motility of microbeads under electric potential was studied using DIC microscopy. Near the polarized electrode, microbeads moved reversibly according to the direction of

applied electric potential, that is, microbeads were attracted to an electrode when the electrode was positively charged (+1.0 V) and were repelled from the electrode when its polarity was changed to negative (-0.5 V) (Figure 2.10). This result verified that the microbeads have negative charge in an aqueous solution.

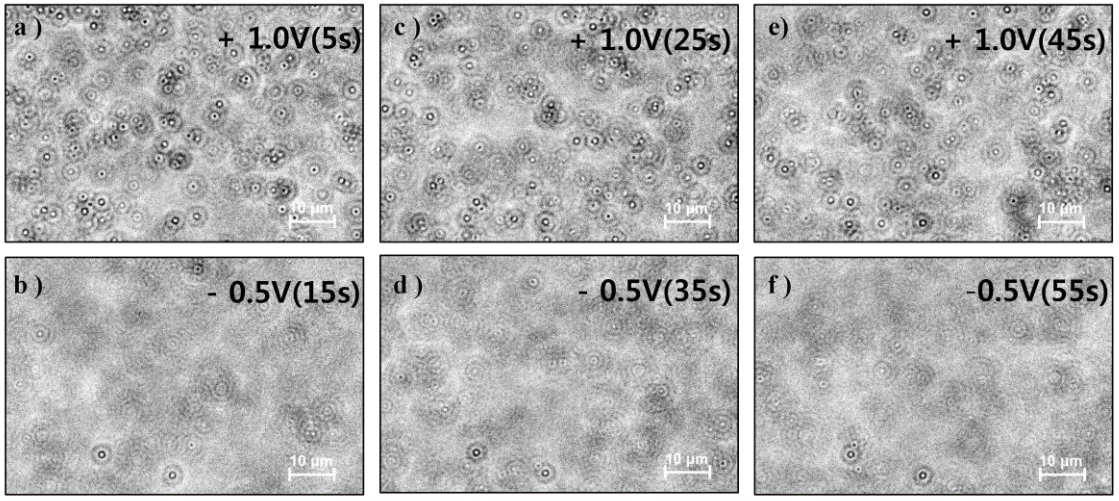

Time(s)	0-10	10-20	20-30	30-40	40-50	50-60
Applied Potential(V)	+ 1.0V	- 0.5V	+ 1.0V	- 0.5V	+ 1.0V	- 0.5V

Figure 2.10 Mobility test of the microbeads under an electric potential. DIC microscope images showing a reversible attraction and repulsion of negatively charged microbeads in the flow cell according to a direction of applied electric potential. The microbeads migrate to the electrode when the electrode gets positively charged, while they are repelled from the electrode when the electrode gets negatively charged. a, b, c, d, e, f) Reversible attraction and repulsion according to the direction of the applied electric field.

2.4.2 Pattering of Microbeads on a Disk Micro-electrode

Reversible patterning of the microbeads on the patterned disk micro-electrode was achieved in this experiment. In the experiment, it was not necessary to form a SAM on

the substrate because microbeads do not typically foul the surface. Figure 2.11 indicates that the microbeads could be patterned on the disk micro-electrode in reversible manner.

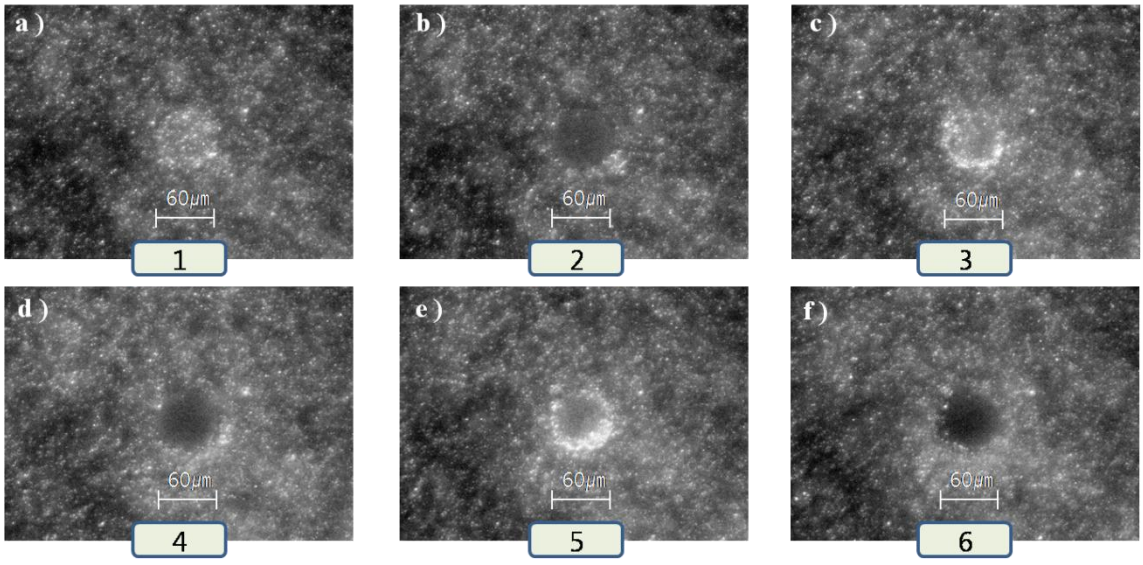

Time(s)	0-10	10-20	20-30	30-40	40-50	50-60
Applied Potential(V)	+ 1.0V	- 0.5V	+ 1.0V	- 0.5V	+ 1.0V	- 0.5V

Figure 2.11 Reversible patterning of the microbeads. Fluorescence microscope images showing a reversible attraction and repulsion of negatively charged microbeads. A disk-microelectrode designed by e-beam lithography was used. The diameter of the disk-microelectrode was 60 µm. a, c, e) The microbeads were attracted to the disk-microelectrode when the electrode was positively polarized. b, d, f) The microbeads were repelled from the disk-microelectrode when the electrode was negatively polarized.

2.4.3 Photobleaching Test

Figure 2.12 shows a photobleaching phenomenon that took place for 10 minutes on the microbeads inside the flow cell under the continuous exposure of excitation light. With time, the measured number of microbeads decreased exponentially. Photobleaching

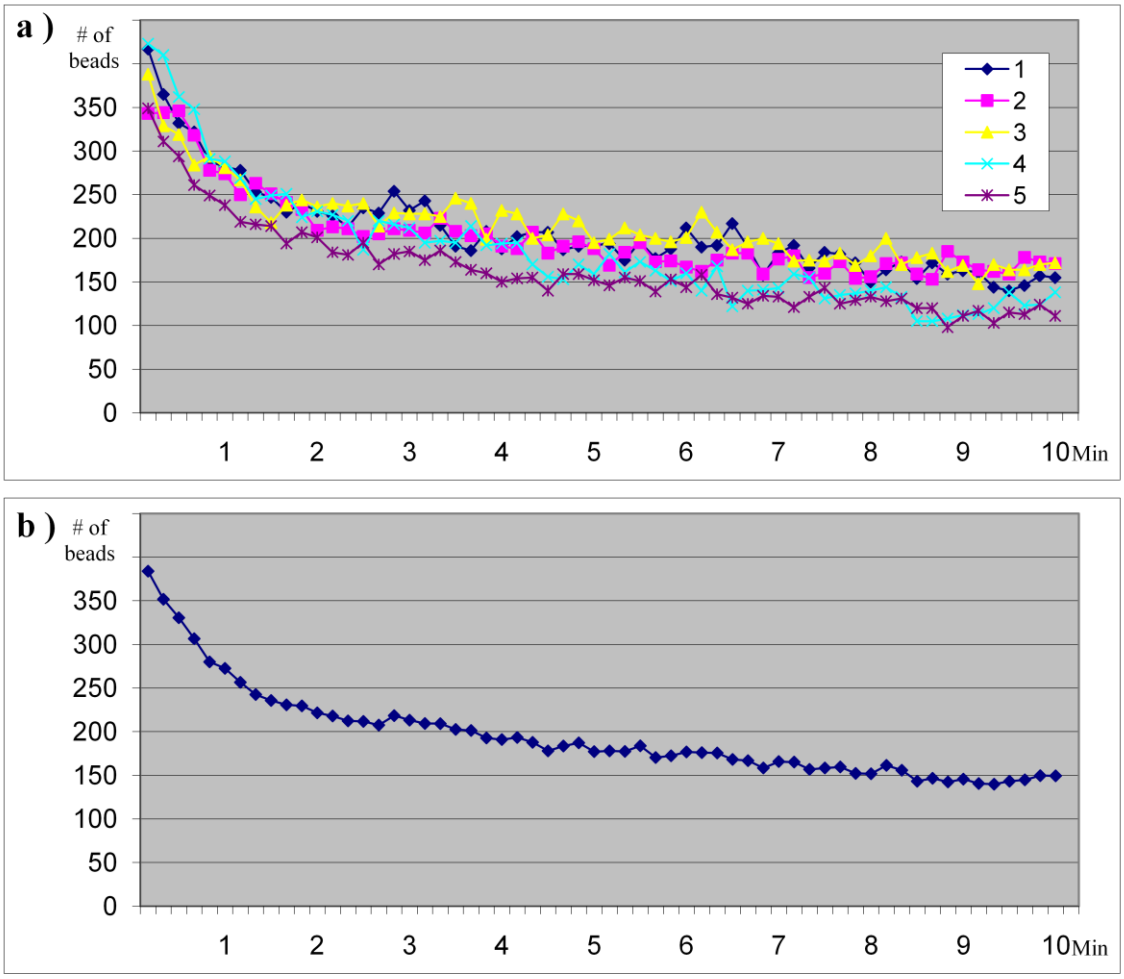

Figure 2.12 Characterization of the photobleaching phenomenon. The photobleaching phenomenon happens in the flow cell under the continuous exposure of excitation light. The exponential decrease in the number of counted microbeads was observed using NIS elements software. a) 5 sets of time series images were taken. For each measurement, new flow cell and fresh microbead solution were used. b) An averaged quantity of the counted microbeads. It shows decay in detected number of microbeads with time.

results in a high decay rate of the number of microbeads counted at the beginning, but the decay rate decreases with time and then eventually becomes almost constant. It takes about 3 minutes to take a set of Z-series images and by closing the shutter, which blocks the excitation light from the light source between image acquisitions, the total exposure

time can be minimized to 30 seconds. If Z-series images were taken from the beginning of the exposure, the photobleaching phenomenon on the microbeads cannot be ignored and the counted number of microbeads would be affected. However, if Z-series images were taken after 5 minutes of exposure, photobleaching can be ignored during the 30 seconds. Through the photobleaching experiment, the standard Z-series image acquisition process

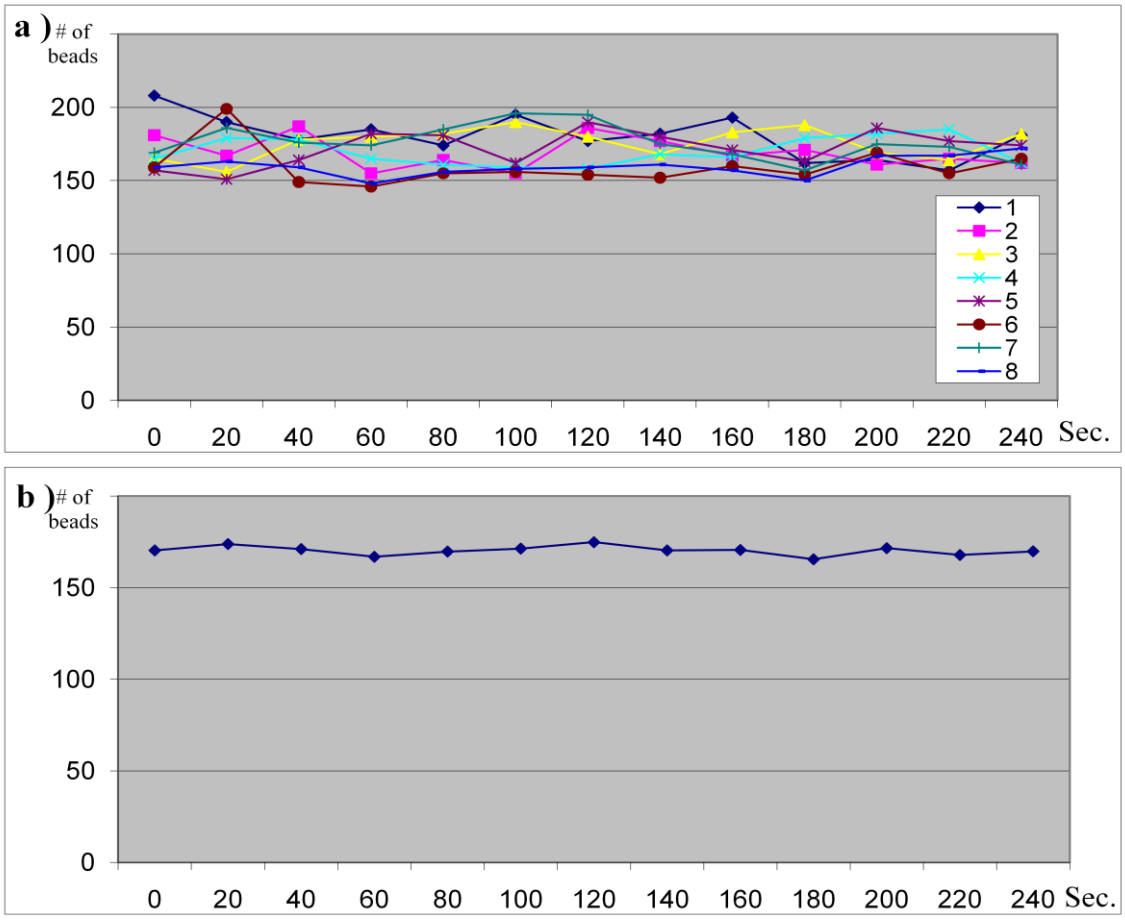

Figure 2.13 Photobleaching test at fixed height. The number of microbeads counted from time-series images taken at a fixed height (the middle of the flow cell). The standard Z-series image acquisition method was used but at a fixed height. a) 8 sets of time series images were taken. For each measurement, new flow cell and fresh microbead solution were used. b) The averaged quantity of the counted microbeads. It shows that photobleaching did not take place during the image acquisition process.

was developed in a manner in which the impact of photobleaching on the final data acquisition would be minimized. As mentioned in the materials and method section for the Z-series image acquisition (subheading 2.3.8), prior to taking images, the flow cell was exposed to excitation light for 5 minutes and during the acquisition the shutter was opened only when images were taken. Figure 2.13 indicates that the photobeaching phenomenon can be ignored in the standard Z-series image acquisition process. In Figure 2.13, the number of microbeads counted from the time-series images taken at the fixed height (the middle of the flow cell) was plotted. For this measurement, the standard Z-series image acquisition method was carried out at fixed height.

2.4.4 Distribution of Microbeads under Influence of Electric Potential

2.4.4.1 Distribution of Microbeads without an Electric Potential

Before examining the distribution of the microbeads under an external electric potential, it should be verified that there are no other factors that would affect the distribution. One possible factor which is likely to have an impact on the distribution is gravity. It can be verified that gravity does not influence the measured distribution by examining the distribution without an external electric potential. The effect of gravity on the distribution of microbeads was investigated and the experimental result is plotted in Figure 2.14. The standard Z-series images were taken and analyzed without application of an external electric potential. The data in the Figure 2.14 indicate that gravity does not have an effect on the distribution of the microbeads.

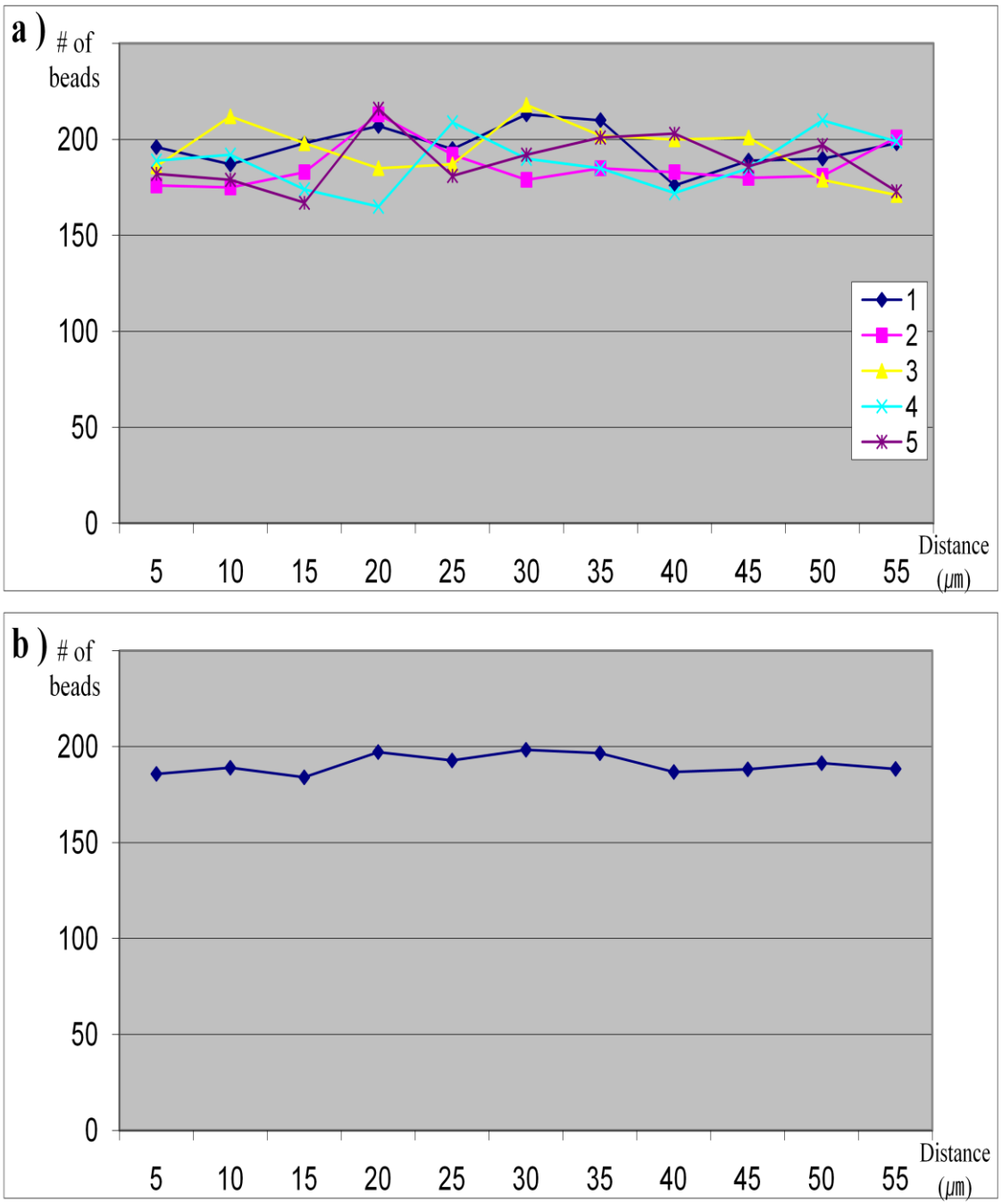

Figure 2.14 Distribution of the microbeads without an electric potential. The possible effect of gravity was investigated without an external electric potential. It was verified that gravity does not have an effect on the distribution of the microbeads. a) 5 sets of Z-series images were taken. b) An averaged quantity of the counted microbeads.

2.4.4.2 Boltzmann Distribution of Microbeads

The number concentration of distributed microbeads inside the flow cell under an external electric potential should follow the Boltzmann distribution.

$$\rho(x) = \rho_0 e^{-\beta\varepsilon} = \rho_0 e^{-\frac{q\phi(x)}{k_B T}}$$

$$\rho(x): \text{number concentration},\ k_B: \text{Boltzmann constant}$$
$$q: \text{effective charge of the microbead},\ \phi(x): \text{electric potential}$$

The number concentration is determined by the product of the effective charge of the microbead and the electric potential at a certain position. For the data in Figure 2.15, 0.4 V was applied between the two planar electrodes comprising the flow cell and two sets of Z-series images were taken and averaged. The graph shows that the number concentration decays exponentially indicating that the distribution of the microbeads under an external electric potential follows the Boltzmann distribution. By taking a logarithm of the number concentration, a linear graph was obtained as shown in Figure 2.16. If one considers a log of the Boltzmann distribution, a linear graph in Figure 2.16 implies that the electric potential inside the flow cell obeys a linear function.

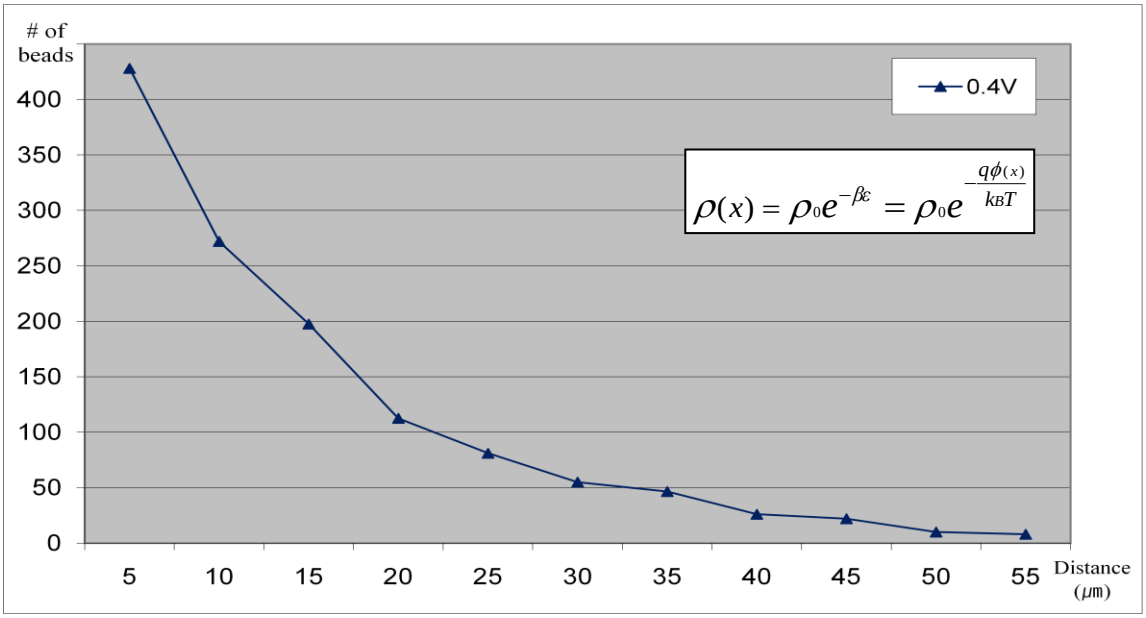

Figure 2.15 The distribution of the microbeads. The distribution of the microbeads under the influence of an external electric potential (0.4V) obeys a Boltzmann distribution. Two sets of Z-series images were taken and averaged.

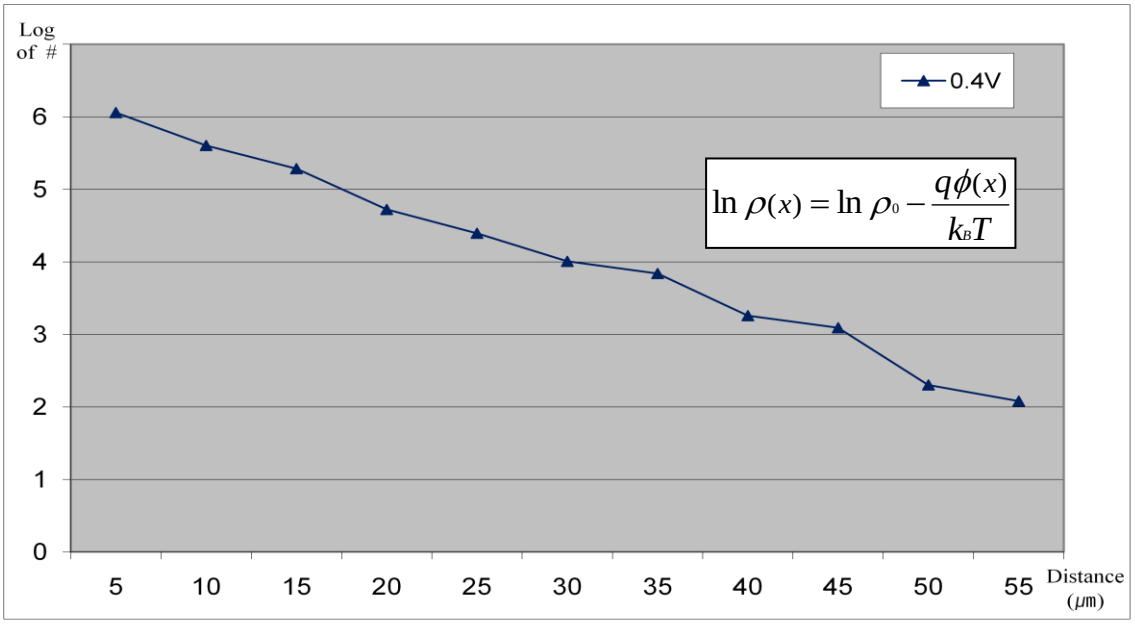

Figure 2.16 Log of the number concentration of the microbeads. 0.4V was applied between two planar electrodes. This graph shows that the electric potential inside the flow cell is almost a linear function with respect to a distance from the electrode.

$$\ln \rho(x) = \ln \rho_0 - \frac{q\phi(x)}{k_B T}$$

By differentiating this function and employing the relation between an electric potential and an electric field, the electric field inside the flow cell can be calculated.

$$\frac{d \ln \rho(x)}{dx} = -\frac{q}{k_B T}\frac{d\phi(x)}{dx} = \frac{q}{k_B T}E(x)$$

By following this mathematical deduction, Figure 2.16 implies that the electric field inside the flow cell is constant and the slope of the graph indicates the value of the product of the effective charge ‘q’ and the electric field ‘E’.

2.4.4.3 Electric Potential Dependence

As explained in the background section (Ch 2.2.1), electrostatic screening takes place on the electrodes and the microbeads. The electrostatic screening results in the reduction of the electric field inside the flow cell and of the effective charge of a microbead. If an external electric potential is applied on a flow cell, ions in the aqueous solution will move to both electrodes depending on their polarity, and this phenomenon will cause a decrease in the electric field inside the flow cell and the increase in the effective charge of a microbead. By examining the distribution of microbeads under different electric potentials, a relationship between ‘qE’ and the applied electric potential can be studied. Figure 2.17 shows the Boltzmann distribution of microbeads under different electric potential from 0.2V to 0.5V. The decay rate of each graph depends on the applied potential.

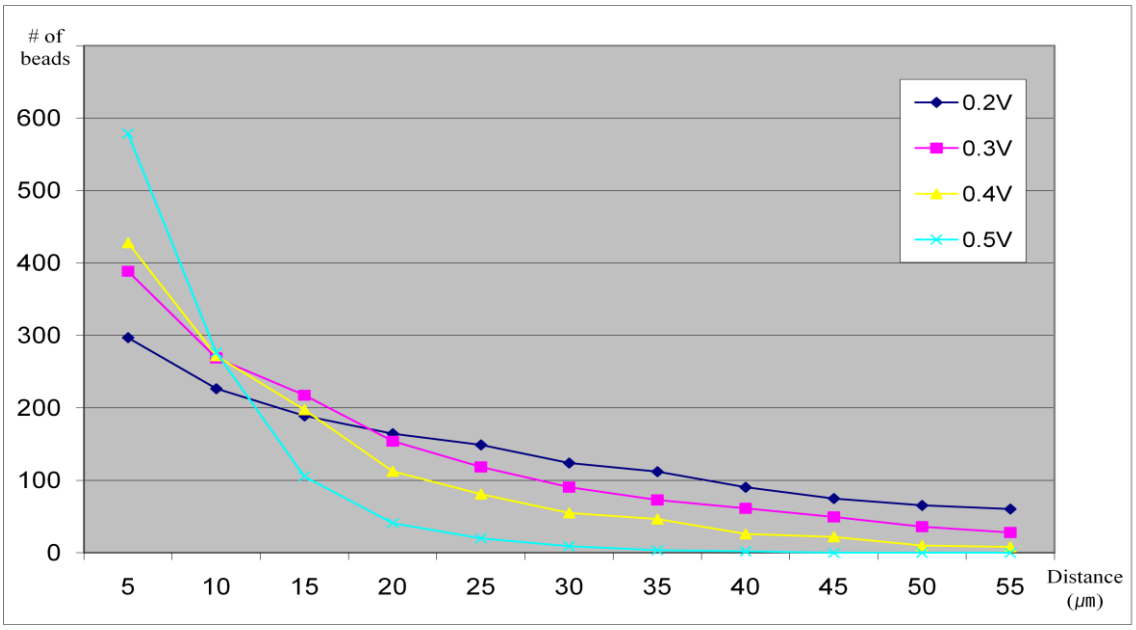

Figure 2.17 Potential dependence of the distribution. The number concentrations of the microbeads under different electric potentials are plotted. Each graph shows the Boltzmann distribution, an exponential decay.

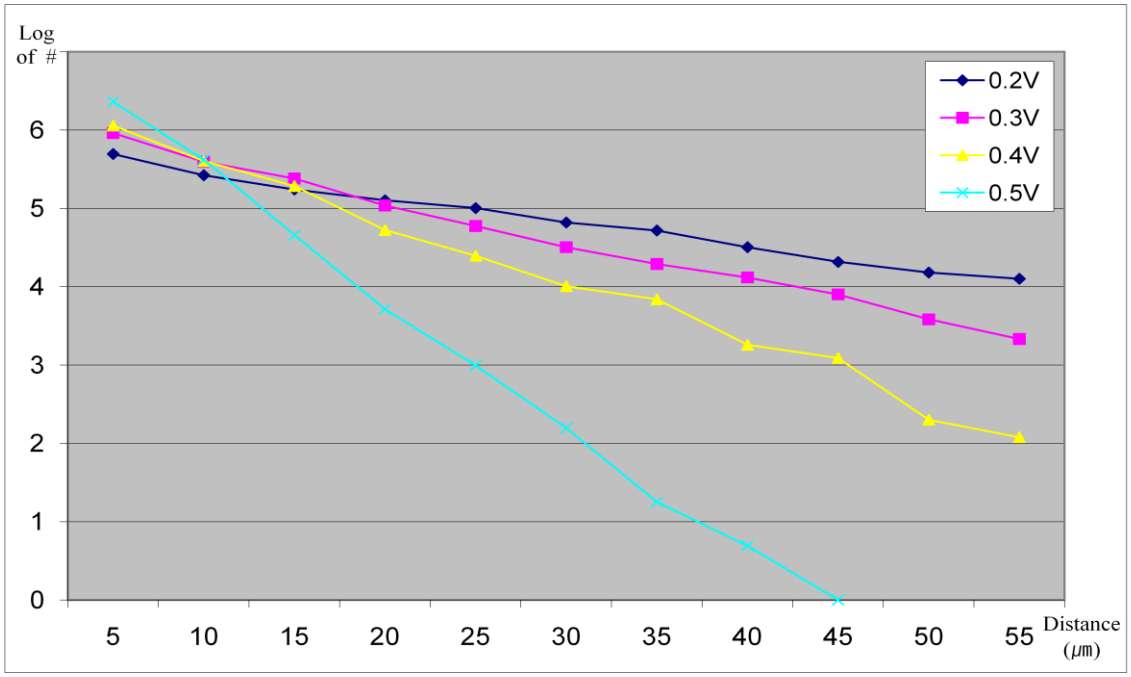

Figure 2.18 Log of the number concentration (potential dependence). Each graph shows a constant slope.

In Figure 2.18, the logarithm of the number concentration shows a constant slope with respect to the distance from the electrode. From Figure 2.18, a product of 'q' and 'E' can be calculated using the slope of each graph.

$$\frac{d\ln\rho(x)}{dx} = -\frac{q}{k_B T}\frac{d\phi(x)}{dx} = \frac{q}{k_B T}E(x)$$

In the above equation, the left side is the slope of the graph and k_BT is a constant which has a value of 0.0256eV at room temperature (25℃). From this equation 'qE' was calculated at different electric potentials (Table 2.3).

Table 2.3 Calculated values for 'qE' from Figure 2.18

	0.2V	0.3V	0.4V	0.5V
qE (eV/m)	799.23	1300.99	2009.6	4143.62

The calculated 'qE' are plotted in Figure 2.19 and it increases exponentially with respect to the applied electric potential. If the electrostatic screening on the electrode and the microbead does not take place, the graph should be a linearly increasing function because the effective charge would be a constant 'q_0' and the electric field would be a linear function with respect to the applied electric potential. However, we have to consider the electrostatic screening on both (1) the electrode and (2) the microbeads to explain Figure 2.19. In the case of (1), accumulated counterions on the electrode would cause electrostatic screening resulting in a decrease of the electric field inside the flow cell. It can be expected that as more electric potential in applied to the electrode, more counterions are accumulated on it and cause stronger screening. As a result, the electric

field will be an increasing function but the rate of increase gets smaller as the applied electric potential is raised. In the case of (2), counterions would cover the microbeads resulting in a decrease of the effective charge of the charged microbeads. If the applied potential increase, less counterions will remain in the bulk of the solution and it leads to an increase of the effecitive charge of the microbeads because screening effects get weakened. Eventually, the product of the effective charge and the electric field is determined by how much the electrostatic screening affects each of them. Based on Figure 2.19, it is plausible to say that the weakening of the screening on the microbead (increase of effective charge) dominates the strengthening of the screening on the electrode (decrease of electric field) as the applied electric potential increases.

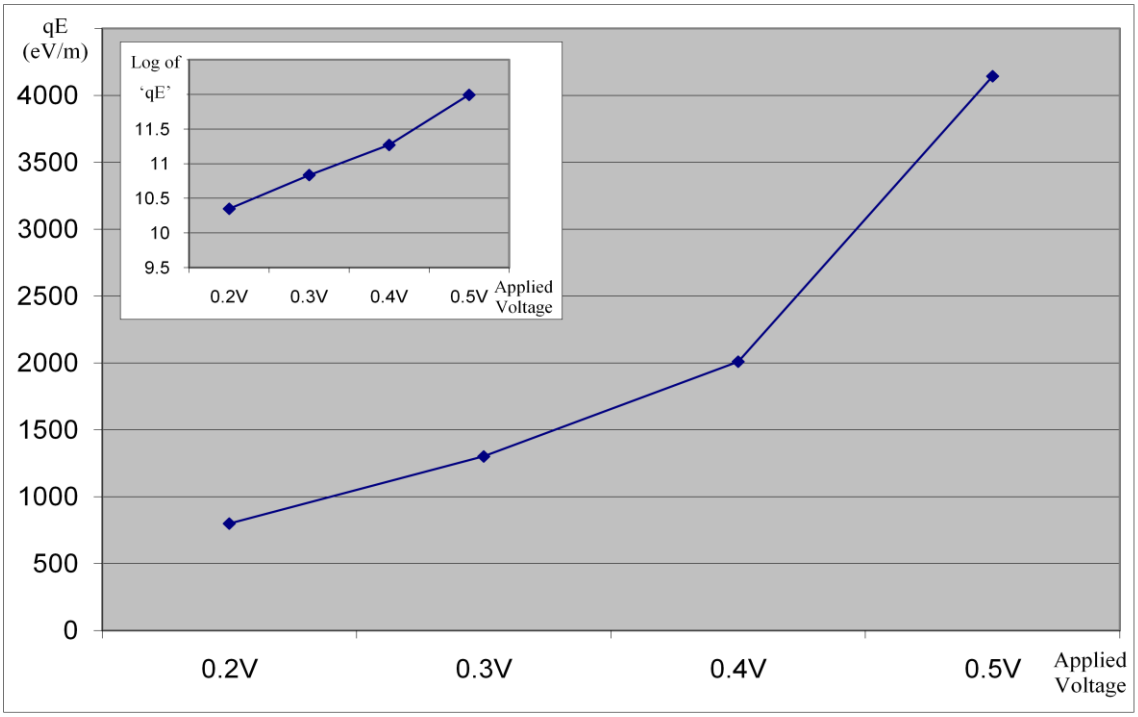

Figure 2.19 Calculated values for 'qE'. It shows that the increase of the effective charge of the microbead dominates the reduction of the electric field inside the flow cell.

2.4.4.4 Time Dependence

The time dependence of the distribution of microbeads is also examined. In order to check the time dependence of the distribution, 5 sets of Z-series images were taken from 10 to 50 minutes in intervals of 10 minutes. For each time measurement, the microbead solution was exposed to an excitation light for 5 minutes prior to taking Z-series images to reduce the photobleaching rate. Figure 2.20 shows the distribution of microbeads under different electric potentials from 0.2V to 0.5V. A remarkable decay in the distribution was observed in the case of higher (0.4V, 0.5V) voltages while only a modest change was observed in the case of the lower voltages (0.2 V, 0.3V). In Figure 2.21, the logarithm of the number concentration illustrates this phenomenon more clearly. When a higher electric potential was applied, a more significant amount of decays in the distribution was observed.

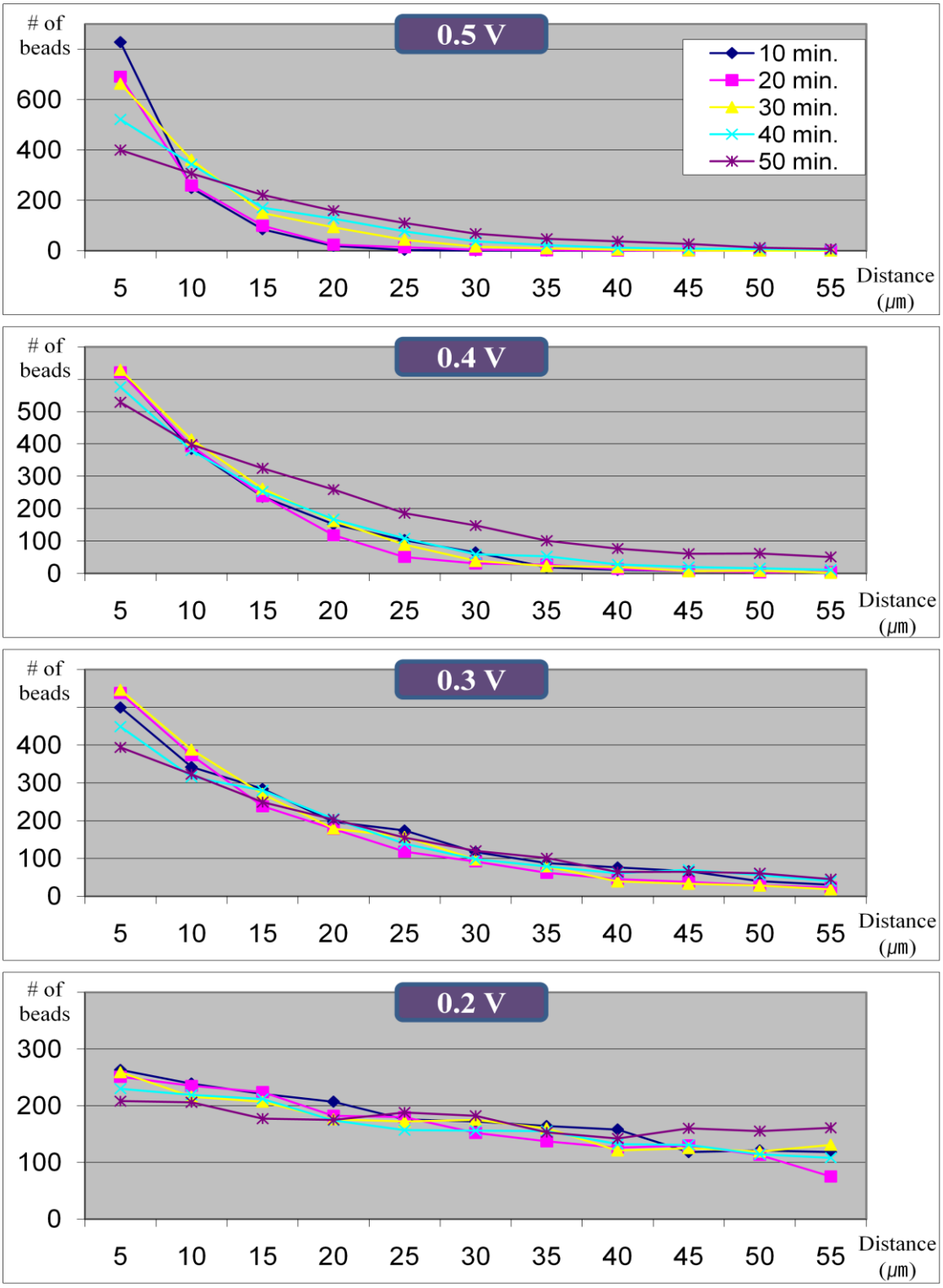

Figure 2.20 Time dependence of the distribution. The number concentrations of the microbeads at different times are plotted.

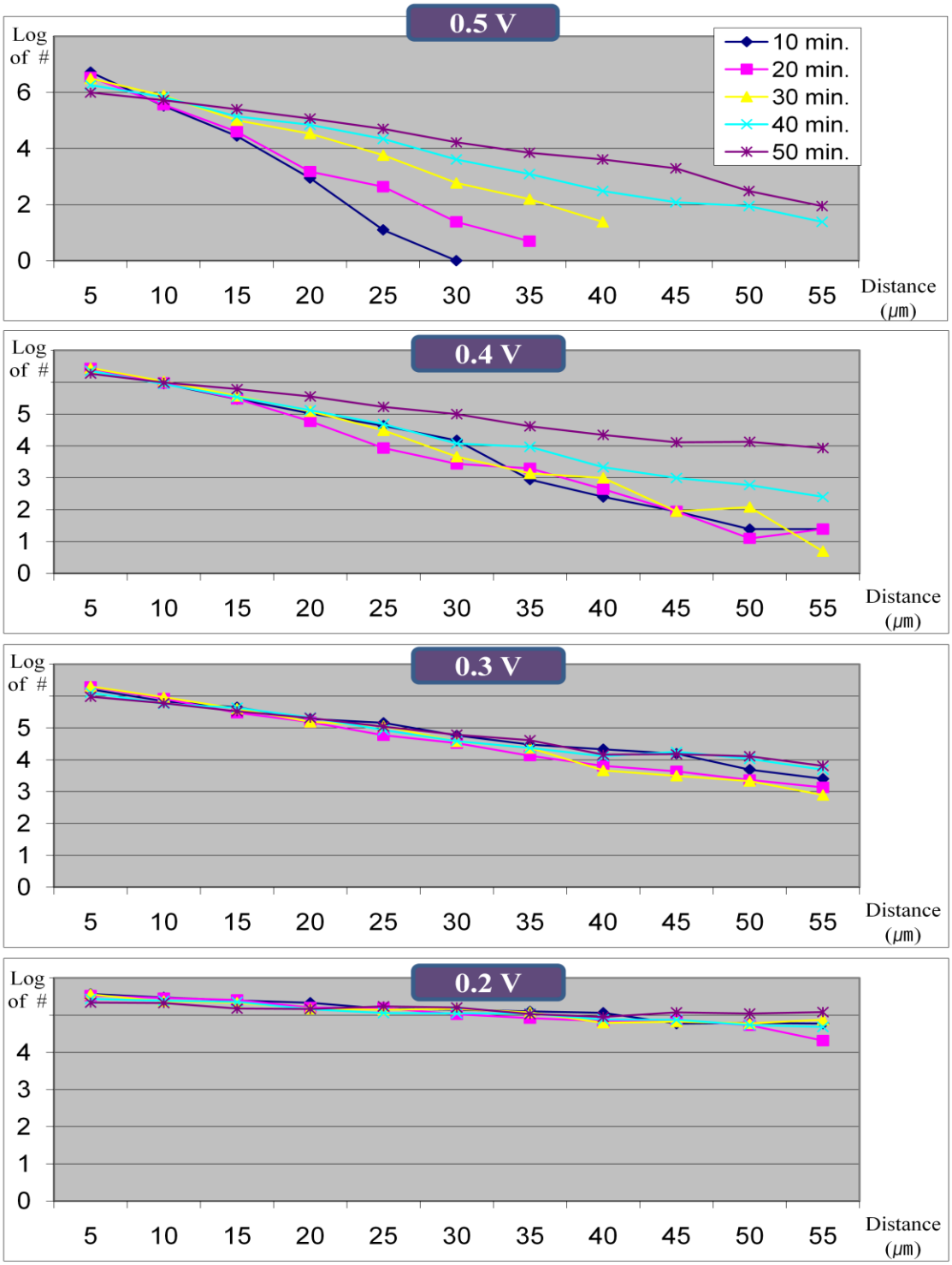

Figure 2.21 Log of the number concentration (Time dependence). When higher electric potentials were applied, the more significant amount of decays in the distribution was observed.

2.5 Conclusion

In this study, an external electric potential is utilized to exert a driving force on charged particles. By applying the external electric potential, the resulting electric field is reduced and the effective charge of the charged particle is increased as a result of the electrostatic screening effect. From the experimental results, it is plausible that a weakening of the screening on the microbeads (increase of the effective charge) dominates a strengthening of the screening on the electrodes (decrease of the electric field) as the applied potential is increased. This phenomenon leads to the conclusion that the driving force does not have a linear relation with the applied electric potential but depends exponentially. In order to utilize the protein manipulation system, self-ionization of water into hydronium and hydroxide ions should be considered because the amount of the self-ionized ions has a decisive effect on the electrostatic screening. As verified in the experiment, above 0.4V, significant dissociation of water molecules into ions takes place and results in decays of both of the electric field and the effective charge of the particles. Therefore, one should be careful in operation of the manipulation system with higher potential.

CHAPTER III

COMPATIBILTY OF ANTIFOULING PROPERTY OF PEG-SAM WITH ELECTRIC FIELD

3.1 Introduction

As previously stated, manipulation of microtubules was achieved to some degree in our laboratory by combining PEG-SAM and electrophoresis. However, so far, it is still limited to bulk patterning of microtubules on a patterned electrode. To achieve single microtubule manipulation in order to construct a bio-track, longer time exposure of an electric potential might be required. Therefore, the compatibility of antifouling properties of a PEG-SAM with electric field should be examined. There are only a few reports related to this topic showing simulation and experimental results.[11-12] Although these previous studies examined the conformational changes of spacer chains and changes of exposed atoms at a surface in a SAM, they did not give an explanation about the direct relation between the antifouling property of the PEG-SAM and the electric field. It was reported that an electric field could lead to disorder of the molecules comprising a PEG-SAM, and this disorder would be related to the direction as well as the magnitude of the applied electric field.[11] This disorder was attributed to changes in the chain conformation, the tilt angle of each chain and the exposed atoms at the surface. These changes in the PEG-SAM might affect hydrophilicity of the surface and this could cause a change in the antifouling properties of the PEG-SAM. In this study, the stability of the antifouling properties of PEG-SAM was studied by examining interactions between the PEG-SAM and the microtubules.

3.2 Background – Antifouling Property of PEG-SAM

SAMs are ultra thin films which are composed of a head group, spacer and functional group. The head group has a special affinity for specific substrates resulting in chemisorption onto the substrate. The nucleated chemisorption expands across the areas of the substrate and, eventually, the adsorbate molecules in the head group cover the entire substrate forming a single monolayer on it. These bonds between the adsorbate molecules and the substrate are very stable because they are covalent. SAMs have been one of the most attention grabbing research areas for last few decades.[13-15] It is because they have various functions according to their functional groups. The properties of a surface can be entirely changed by SAMs, although they have only a few nanometers of thickness. One of the widely utilized functionalities is the antifouling property of the PEG-SAM. A PEG-SAM is a SAM with poly(ethylene glycol) chains as functional groups with alkyl termination. It has been revealed that PEG-SAMs have protein resistance and have been used to functionalize a surface to have antifouling properties by several groups.[16-17] The protein resistance can be changed by the length of the PEG chains and the alkyl termination because they have an effect on the internal and terminal hydrophilicity. The lateral packing density and temperature also can have an influence on the protein resistance of the PEG-SAM. In this study, 2-[methoxypoly-(ethyleneoxy)propyl]-trimethoxysilane (MPEOPS) was used and MPEOPS was verified to have a reasonable antifouling property against microtubules in our previous study.[6]

3.3 Materials and Methods

3.3.1 Electrode Preparation

In order to test the compatibility of the antifouling properties of the PEG-SAM, a disk micro-electrode and a transparent electrode were used as the top and bottom electrodes respectively. By using the patterned electrodes, the difference between the region exposed to the electric field and the region not exposed to the electric field can be compared. To fabricate the disk micro-electrode and the transparent electrodes, e-beam lithography and thermal evaporation were utilized as discussed in subheading 2.3.2 and subheading 2.3.3.

3.3.2 PEG-SAM Formation

To form a PEG-SAM layer on the silicon wafer where the disk micro-electrode was fabricated, the protocol developed in our previous research was used.[6] 2-[methoxypoly-(ethyleneoxy)propyl]-trimethoxysilane (MPEOPS), 95%, was purchased from Gelest, Inc. It was mixed with toluene to make a concentration of 5% v/v, and stirred for 1 minute. In order to protect the silane molecules from reacting with water molecules in solution and forming a facile polymer in it, the stirring process should be very gentle. This is because violent mixing might cause dissolution of water vapor from the atmosphere into the solution resulting in incomplete polymerization of silane molecules in the solution.[13] After making the solution, patterned silicon wafers were placed in a glass beaker which were then submerged in 20mL of the prepared SAM solution. The

beaker containing the substrates and the solution was heated in a well-ventilated oven to 75 °C for 21 hours. The substrates were then thoroughly rinsed with toluene and isopropanol and dried with nitrogen gas.

3.3.3 Flow Cell Preparation

The flow cell preparation procedure described in subheading 2.3.4 was utilized.

3.3.4 Exposure to E-field

After making the flow cell, the two electrodes were connected to a power supply and an electric potential was applied between them. In this manner, the PEG-SAM on the patterned disk micro-electrode was exposed to the applied electric potential. An electric potential of 1.0V was applied for an hour where positive potential means that the disk micro-electrode was polarized positively. The test was repeated in two different ways, for one test the flow cell was filled with DI water during the application of the E-field and in the second test the flow cell was left empty.

3.3.5 Microtubule Preparation

To verify the antifouling property of the PEG-SAM, microtubules were used because it was verified that the PEG-SAM has reasonable antifouling properties to microtubules in our previous research.[6] The microtubule preparation protocol of the lab of Tim Mitchison at Harvard was used in this study [source; http://mitchison.med.harvard.edu/protocols/poly.html]. Briefly, rhodamine labeled

tubulin (50 μM) was mixed with unlabeled tubulin (50 μM) at a ratio of 1:2 in PIPES buffer (80mM Piperazine, 1mM MgCl2, 1mM EGTA, pH 6.8 with KOH) containing 5% glycerol and 1μM GMPCPP. The tubulin was allowed to polymerize at 37ºC for 30 minutes then diluted to a concentration of 0.5 μM in PIPES buffer supplemented with 20 μM taxol. Before each assay, the oxygen scavenging cocktail (glucose 45 mg/mL, glucose oxidase 2 mg/mL, catalase 0.35 mg/mL, 2-mercaptoethanol 5 % v/v in PIPES buffer) was freshly prepared and added to the MTs to prevent depolymerization from fluorescence excitation. The final tubulin concentration used was 0.45 μM.

3.3.6 Antifouling Property Assay Using Microtubules

After exposing the PEG-SAM to the electric field, the power supply was turned off and the two electrodes were short-circuited by attaching two wires on each electrode. Microtubules in the buffer solution were introduced to the flow cell to verify the compatibility of the antifouling property of the PEG-SAM with electric field. After introducing microtubules in the flow cell, it was sealed with vacuum grease and left for 5 minutes to allow microtubules to adsorb on the PEG-SAM. An image of microtubules adsorbed on the electrically treated PEG-SAM was taken by using fluorescence microscopy.

3.4 Results and Discussion

In both cases, with DI water and without DI water during the exposure to the E-field, some of the microtubules were stuck on the PEG-SAM which had been exposed to the

electric potential for 1 hr (Figure 3.1). These results imply that some changes in the PEG-SAM caused by electric potential might result in a loss of the antifouling properties of the PEG-SAM but that the presence of DI water during the application of the potential is not important. There are various possible speculations for this result. (1) Physical disorder (tilt angle of chains, flatness of the surface, segregation of molecules from the substrate, etc.) of molecules composing the PEG-SAM was likely to happen. (2) Atoms which are exposed to the surface of the PEG-SAM could be changed and this can have an effect on the hydrophilicity of the PEG-SAM. (3) Conformational changes of the chain may take place and this also can influence the hydrophilicity of the PEG-SAM. Although it was observed that the antifouling property of the PEG-SAM was damaged by the electric potential, it is hard to explain what exactly happened on the PEG-SAM and why they lost their antifouling property.

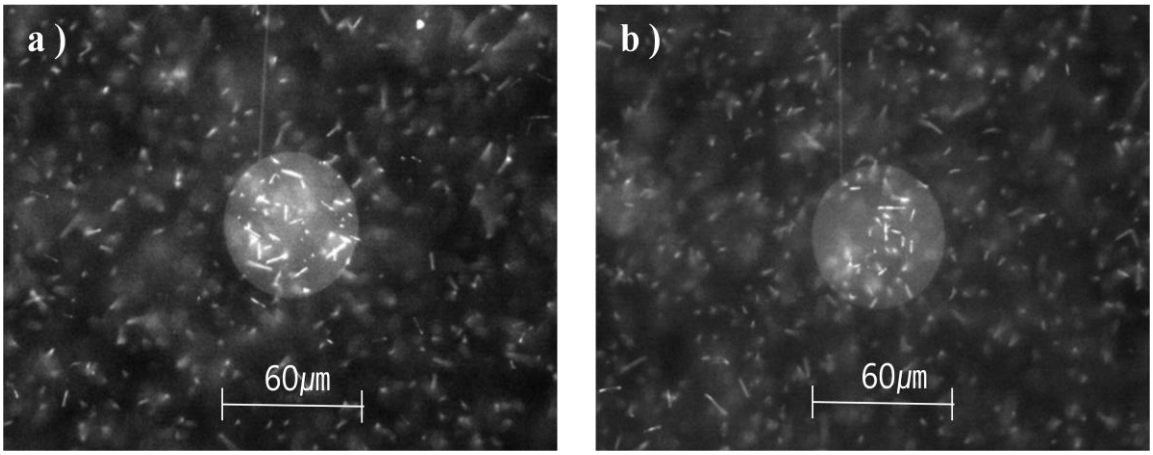

Figure 3.1 Adsorption of microtubules on the electrically treated PEG-SAM. The adsorbed microtubules on the PEG-SAM on the disk-microelectrode were observed by a fluorescence microscope after exposure to an electric potential. a) The flow cell was filled with DI water when it had been exposed to the electric potential. b) The flow cell wasn't filled with DI water when it had been exposed to the electric potential.

3.5 Conclusion

In this chapter, the compatibility of an antifouling property of the PEG-SAM with an electric field was examined. From the results, it becomes clear that the antifouling property of the PEG-SAM cannot be retained after an exposure to the electric field. However, it is hasty to conclude that the antifouling property of the PEG-SAM is not compatible with an electric field, because, in this research, conditions for the experiment were not systematically studied. Nevertheless, the results from this experiment raise a question about the compatibility of the antifouling property of the PEG-SAM with an electric field. To verify the compatibility, more systematic experiments varying the conditions for the exposure of the electric field on the PEG-SAM should be carried out. Furthermore, in order to investigate what happens on the PEG-SAM upon exposure of an electric field, various characterization methods can be used such as contact angle measurement, ellipsometry, X-ray photoelectron spectroscopy (XPS), secondary ion mass spectrometry (SIMS), Fourier transform infrared spectroscopy (FT-IR) and atomic force microscopy (AFM).

CHAPTER IV

SUMMARY

Techniques for the immobilization of bio-molecules on a specifically designed area have been one of the challenging research areas of bio and life scientists. It is of interest because of the applicability not only to bio-engineering but also to basic scientific research.

In our previous research, fabrication of microtubules has been achieved by combining PEG-SAMs and electrophoresis. The PEG-SAM is used for functionalizing the silicon wafer surface to have antifouling properties and electrophoresis is employed to exert a driving force to move microtubules. Although bulk manipulation of the microtubules was achieved by the patterning system in the previous research, it had to be characterized in more detail to improve the manipulating resolution.

In this study, the previously performed electrically-guided protein patterning system incorporating antifouling self-assembled monolayers was characterized to understand dynamics of the charged particles and stability of the PEG-SAM under an externally exerted electric potential. Microbeads were used as a model charged particles and DIC and fluorescence microscopy was utilized to observe them.

To understand the dynamics of the charged particles between two polarized electrodes filled with an aqueous solution where electrostatic screening takes place, the distribution of the microbeads under an electric potential was analyzed using the Boltzmann distribution. By analyzing the distribution of the microbeads, it is shown that

the driving force which is the product of the electric field and the effective charge of the charged particle does not have a linear relation with the applied electric potential but an exponentially increasing function with respect to the potential. The cause may be that a weakening of the screening on the charged particles (increase of the effective charge) dominates a strengthening of the screening on the electrodes (reduction of the electric field) as the applied potential is increased. It also has been shown that, above 0.4V, significant dissociation of water molecules into hydronium and hydroxide ions takes place and results in decays of both the electric field and the effective charge of the particles. This experimental result indicates that the pattering system should be operated in the potential regime where dissociation of the water molecules does not occur.

To make the protein patterning system useful, the compatibility of the antifouling property of the PEG-SAM with an electric field had to be verified. In this study, the antifouling property of the PEG-SAM was not retained after an exposure to the electric field. However, more systematic experiments varying the conditions for the exposure of the electric field on the PEG-SAM should be carried out. Furthermore, various characterization methods can be used to characterize PEG-SAMs after exposure to an electric field such as a contact angle measurement, ellipsometry, X-ray photoelectron spectroscopy (XPS), secondary ion mass spectrometry (SIMS), Fourier transform infrared spectroscopy (FT-IR) and atomic force microscopy (AFM).

REFERENCES

1. Christman, K. L.; Enriquez-Riosa, V. D.; Maynard, H. D. *Soft Matter* **2006,** *2*, 928-939.
2. Yebra, D. M.; Kiil, S.; Dam-Johansen, K. *Progress in Organic Coatings* **2004**, *50*, 75-104.
3. Hyun, J.; Ahn, S. J.; Lee, W. K.; Chilkoti, A.; Zauscher, S. *Nano Lett.* **2002**, *2*, 1203-1207.
4. Kannan, B.; Castelino, K.; Chen, F. F.; Majumdar, A. *Biosens. Bioelectron.* **2006**, *21*, 1960-1967.
5. Lan, S.; Veiseh, M.; Zhang, M. *Biosens. Bioelectron.* **2005**, *20*, 1697-1708.
6. Noel, J. A.; Teizer, W.; Hwang, W. *ACS Nano* **2009**, *3*, 1938-1946.
7. van den Heuvel, M. G. L.; Dekker, C. *Science* **2007**, *317*, 333-336.
8. Khripin, C.; Jagota, A.; Hui, C.Y. *J. Chem. Phys*. **2005**, *123*, 134705-1-134705-11.
9. Denton, A. R. *Physical Review E* **2004**, *70*, 031404-1-031404-18.
10. Tanaka, M.; Grosberg, A. Y. *Eur. Phys. J. E* **2002**, *7*, 371-379.
11. Vemparala, S.; Kalia, R. K.; Nakano, A.; Vashishta, P. *J. Chem. Phys.* **2004**, *121*, 5427-5433.
12. Lahann, J.; Mitragotri, S.; Tran, T. N.; Kaido, H.; Sundaram, J.; Choi, I. S.; Hoffer, S.; Somorjai, G. A.; Langer, R. *Science* **2003**, *299*, 371-374.
13. Ulman, A. *Chem. Rev.* **1996**, *96*, 1533-1554.

14. Onclin, S.; Ravoo, B. J.; Reinhoudt, D. N. *Angew. Chem. Int. Ed.* **2005**, *44*, 6282-6304.

15. Ariga, K.; Nakanishi, T.; Michinobu, T. *J. Nanosci. Nanotechnol.* **2006**, *6*, 2278-2301.

16. Herrwerth, S.; Eck, W.; Reinhardt, S.; Grunze, M. *J. Am. Chem. Soc.* **2003**, *125*, 9359-9366.

17. Prime, K. L.; Whitesides, G. M. *J. Am. Chem. Soc*. **1993**, *115*, 10714-10721.

VITA

Name:	Jinseon Park
Address:	Physics Dept., Texas A&M University College Station, TX 77843-4242
Email Address:	c15044@gmail.com
Education:	B.S., Physics, Korean Military Academy, 2006